Phage-delivered CRISPR-Cas9 for strain-specific depletion and genomic deletions in the gut microbiota

Kathy N. Lam[1], Peter Spanogiannopoulos[1], Paola Soto-Perez[1], Margaret Alexander[1], Matthew J. Nalley[1], Jordan E. Bisanz[1], Feiqiao B. Yu[2], Peter J. Turnbaugh[1,2,*]

1 Department of Microbiology and Immunology, University of California San Francisco, USA
2 Chan-Zuckerberg BioHub, San Francisco, USA
* Correspondence to: Peter.Turnbaugh@ucsf.edu

Abstract

The recognition that the gut microbiome has a profound influence on human health and disease has spurred efforts to manipulate gut microbial community structure and function. Though various strategies for microbiome engineering have been proposed, methods for phage-based genetic manipulation of resident members of the gut microbiota *in vivo* are currently lacking. Here, we show that bacteriophage can be used as a vector for delivery of plasmid DNA to bacteria colonizing the gastrointestinal tract, using filamentous phage M13 and *Escherichia coli* engrafted in the gut microbiota of mice. We employ M13 to deliver CRISPR-Cas9 for sequence-specific targeting of *E. coli* leading to depletion of one strain of a pair of fluorescently marked isogenic strains competitively colonizing the gut. We further show that when mice are colonized by a single *E. coli* strain, it is possible for M13-delivered CRISPR-Cas9 to induce genomic deletions that encompass the targeted gene. Our results suggest that rather than being developed for use as an antimicrobial in the gut microbiome, M13-delivered CRISPR-Cas9 may be better suited for targeted genomic deletions *in vivo* that harness the robust DNA repair response of bacteria. With improved methods to mitigate undesired escape mutations, we envision these strategies may be developed for targeted removal of strains or genes present in the gut microbiome that are detrimental to the host. These results provide a highly adaptable platform for *in vivo* microbiome engineering using phage and a proof-of-concept for the establishment of phage-based tools for a broader panel of human gut bacteria.

Introduction

Broad interest in the influence that the gut microbiome has on host health and disease has led to the development of strategies with which to manipulate the structure and function of host-associated microbial communities. Various approaches for microbiome modification have recently been described, including engrafting bacterial strains in a naive host by providing exclusive nutrient sources in the diet [1, 2] or treating with antibiotics [3, 4]; introducing transient bacteria as a live therapeutic to complement an absent host metabolic activity [5, 6]; and chemically inhibiting microbial pathways active in host disease states [7] or drug-induced toxicity [8]. Bacteria have also been engineered to respond *in vivo* (within the gut) to dietary compounds and synthetic inducers [9, 10], as well as to deliver genetic payloads to diverse members of the gut microbiota [11] or to target multi-drug resistant opportunistic pathogens [12]. Current strategies for microbiome editing, however, either lack species- or strain-level precision or require the introduction of an exogenous bacterium into the host. A valuable and complementary strategy is the genetic manipulation of members of the gut using more specific tools to target bacteria for genome modification *in vivo*.

Although bacterial viruses (bacteriophage or phage) have a long history of use in phage therapy [13–17], these applications have generally focused on the clearance of bacterial pathogens and made use of phages in their native form. In the case of *E. coli*, the use of coliphages to target the bacterium in the gut of mice suggested that eradication or permanent depletion may be complicated by factors that include the emergence of phage resistance, protective effects of the gut environment that allow phage-sensitive cells to persist, or changes in bacterial physiology that may impact phage infection *in vivo* [18–21]. An example of the latter are the phase-variable capsules of the gut bacterium *Bacteroides thetaiotaomicron* that lead to varying phage susceptibilities [22]. More recently, the discovery of CRISPR-Cas (endonuclease-containing systems able to generate breaks in nucleic acid at targets defined by CRISPR guide sequences) has enabled the engineering of phage programmed to cleave the DNA of pathogens. For example, engineered phage carrying CRISPR-Cas9 have been used in models of infection for sequence-specific targeting of enterohemorrhagic *E. coli* in moth larvae and antibiotic-resistant *Staphylococcus aureus* on mouse skin [23–25]. Engineered phage carrying only the CRISPR guide sequences have also been used against pathogenic *C. difficile* in the mouse gut and function by hijacking the bacterium's endogenous CRISPR-Cas3 system [26]. The sheer diversity of phages existing in nature, the ease with which they can be isolated against a wide range of bacteria, and their natural abundance [27, 28] make them attractive agents to engineer for gene delivery to bacterial cells colonizing the gut. Despite the huge potential of phages in this respect, there is currently a lack of *in vivo* models with which to study genetically tractable pairs of phages and their bacterial hosts specifically in the context of genetic editing of a commensal microbe within an established host-associated microbial community. Given the complexities and challenges of the mammalian gut environment, the possibility of harnessing phage and CRISPR-Cas9 for gut microbiome editing may be best explored with highly controlled, molecular mechanistic experiments using a reductionist tripartite model system of *E. coli*, a coliphage, and mouse model [29].

Isolated nearly six decades ago from wastewater [30], M13 is a ssDNA filamentous phage belonging to the Inoviridae family in the ICTV classification of viruses [31] and has an interesting life cycle in which it replicates and releases new virions from the cell without causing lysis [32]. It can infect *E. coli* and related Enterobacteriaceae carrying the F sex factor that encodes proteins forming the conjugative F pilus (strains designated as F+, F', or Hfr) [33, 34]. M13 has made impressive contributions to the field of molecular biology — from the development of M13-based vectors for cloning, sequencing, and mutagenesis [35–37] to its application in phage display [38, 39] — making it a very well characterized phage with excellent resources. In particular, the development of phagemid vectors that have both a plasmid origin of replication and an origin for packaging by M13 (*e.g.*, ColE1 and f1, respectively) combine the advantages of plasmid DNA manipulation using standard techniques with the ability to easily package recombinant DNA into virions and generate phage preparations of high titer. Furthermore, the recent appreciation that inoviruses are prevalent in nature and have phylogenetically diverse hosts [40] suggests that M13 could be a useful model for extending to other bacterial species in the gut.

Phage M13 has been used previously in mice; for example, phage-displayed random peptide libraries have been screened in mice to identify “homing” peptides able to target organs or tumours [41–43]. M13 has also been applied by intraperitoneal injection as a bactericidal agent against *E. coli* by engineering it to deliver constructs that encode toxins lethal to the cell [44] or suppressors of the cellular response to DNA damage to enhance the efficacy of bactericidal antibiotics [45]. Of relevance to the gut microbiome, M13 phage displaying antibody variable fragments against *Helicobacter pylori* surface antigens have been shown to reduce colonization by the bacterium in the mouse stomach when bacteria are pretreated with phage before oral inoculation [46], and M13 carrying CRISPR-Cas9 have been used as an antimicrobial in a larval model of bacterial infection [23]. However, the use of M13 to deliver genetic constructs to established cells in the complex environment of the mammalian gastrointestinal tract for maintenance in the host has not been demonstrated, nor has its use as phage chassis for delivery of a CRISPR-Cas system to cells residing in the mouse gut. Here, we employ the established streptomycin-treated mouse model to stably engraft *E. coli* among the microbiota [4, 47–49] and demonstrate that M13 can be used to deliver phagemid DNA to *E. coli* cells in the mouse gut, and further apply this strategy to deliver phagemid vectors carrying CRISPR-Cas9 to manipulate strain composition as well as the genomic content of cells *in vivo*.

Results

Phage M13 can be used to deliver DNA to *E. coli* in the gut

To test whether we could deliver plasmid DNA via M13 to *E. coli* colonizing the gut, we turned to the existing phagemid pBluescript II [50]. We made use of the *bla* gene (encoding beta-lactamase) carried on this vector, which confers resistance to beta lactam antibiotics, reasoning that successful delivery to *E. coli* in the gut could be selected for using a beta-lactam in the drinking water of mice. Previous studies on the fate of orally administered antibiotics in animals showed that the beta lactam antibiotic ampicillin is poorly absorbed in the small intestine leading to the majority of the drug entering the cecum of rats and large intestine of lambs [51, 52], that resistant strains could be selected for when the antibiotic was provided [53, 54], and that mice will tolerate a concentration of 1 mg/ml in the water [55]. We determined that pBluescript II confers *in vitro* resistance to ampicillin and the semi-synthetic analogue carbenicillin at concentrations exceeding 1 mg/ml while sensitive strains displayed growth inhibition at concentrations 1 to 2 orders of magnitude lower (Figure S1).

To determine whether a resistant subpopulation could be selected for in the gut using a beta-lactam antibiotic in the water, we turned to the streptomycin-treated mouse model; although streptomycin treatment decreases bacterial diversity (Figure S2), it remains a useful model for experimentation with *E. coli* in the mammalian gut. We put mice on water containing streptomycin to prepare for colonization, and subsequently introduced a Sm^{R} *E. coli* population that was a mixture of 99.9% Amp^{S} (no plasmid) and 0.1% Amp^{R} cells (pBluescript II); mice were then split into 2 groups and maintained on water containing only streptomycin (5 mg/ml) or streptomycin and ampicillin (5 mg/ml and 1 mg/ml, respectively) (Figure 1a). We tracked both total *E. coli* and Amp^{R} *E. coli* in mouse feces for 8 days. At 6 hours post-*E. coli* introduction, the percentage of Amp^{R} *E. coli* in the feces of all mice was at or close to 0.1%, consistent with the gavaged mixture transiting through the gastrointestinal (GI) tract. Within 1 to 2 days, however, mice on water containing ampicillin exhibited an increase in the percent of Amp^R *E. coli* by 3 orders of magnitude, reaching complete or near complete colonization by Amp^R cells, whereas the Amp^R subpopulation was lost in mice treated with water containing only streptomycin (Figure 1a). These results demonstrate that a beta lactam antibiotic can be used in the drinking water to select for resistant *E. coli* in combination with the streptomycin model without impacting overall *E. coli* colonization levels, which are very reproducible in this system averaging 10^9–10^{10} CFU per gram feces (Figure 1a).

After confirming that beta lactam-resistant *E. coli* could be selected for using antibiotic in the drinking water, we next wanted to determine how effective beta lactam selection was against a sensitive population of *E. coli*— that is, whether selection could eradicate *E. coli* that had established stable colonization in the mouse gut. A previous study found that a single high dose of ampicillin effected a decrease in the resident sensitive *E. coli* from 10^8–10^9 to 10^5–10^6 CFU per gram feces [52] while another study reported the emergence of spontaneous resistant mutants of *E. coli* under ampicillin selection *in vivo* [56]. Because either of these two scenarios — a high background of sensitive cells or the emergence of spontaneous resistant mutants — could potentially hinder our strategy of using phage to deliver constructs to cells in the gut, we asked whether they could occur in our system. To determine the effectiveness of beta lactam selection against sensitive *E. coli*, we colonized mice with two different Sm^R strains (*E. coli* MG1655 and W1655 F+) and tracked colonization levels during treatment with the beta lactam antibiotic carbenicillin in an alternating exposure regimen lasting 17 days (Figure 1b); carbenicillin was used here and all subsequent experiments for its increased stability over ampicillin. When colonized mice were introduced to carbenicillin (1 mg/ml) in the drinking water, *E. coli* levels dropped 6 to 7 orders of magnitude from 10^9–10^{10} to 10^3–10^4 CFU per gram feces in the first day, and levels decreased to below the limit of detection (approximately 10^2 CFU per gram) over the course of

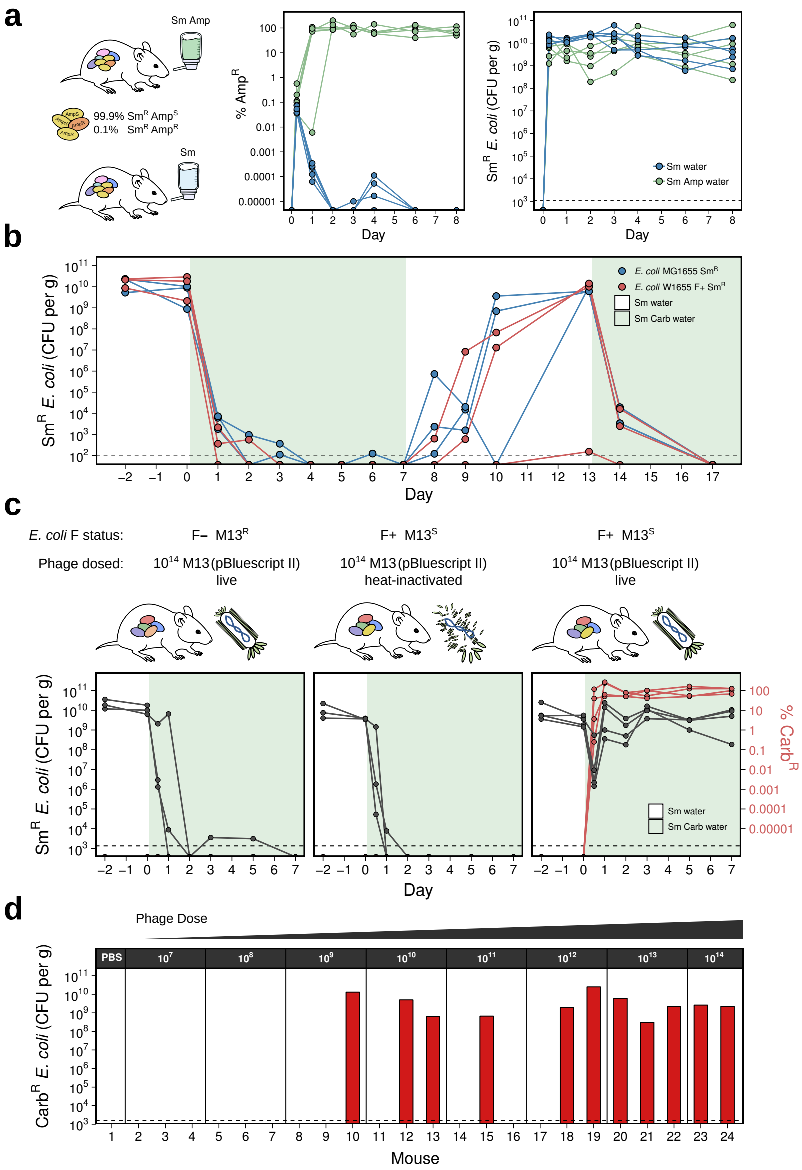

Figure 1. M13 phage can deliver a plasmid-borne antibiotic resistance gene to *E. coli* cells in the mouse gut using the streptomycin treatment model for engrafting *E. coli* in mice. (a) A resistant subpopulation of *E. coli* can be selected for in the gut when a beta lactam antibiotic is provided in the drinking water. Mice were orally gavaged with a mixture of Sm^{R} *E. coli* MG1655 containing 99.9% Amp^{S} cells and 0.1% Amp^{R} cells (Amp^{R} conferred by the plasmid pBluescript II). Mice were then started on water containing only streptomycin (n = 5) or water containing both streptomycin and ampicillin (n = 6). Percent Amp^{R} and total *E. coli* in mouse fecal pellets were determined on MacConkey agar with antibiotic selection. **(b)** A sensitive *E. coli* population is unable to maintain colonization in the gut when the beta lactam antibiotic carbenicillin is provided in the water. Mice were colonized with either Sm^{R} MG1655 or Sm^{R} W1655 F+ (n = 3 per strain) using streptomycin in the water. Carbenicillin was added to the water on Day 0, removed on Day 7, and added again on Day 13. Sm^{R} CFU per gram feces was determined on MacConkey agar with antibiotic selection. **(c)** M13 phage carrying pBluescript II can infect F+ *E. coli* in the gut. Mice were split into three experimental groups: (1) colonized with Sm^{R} W1655 F− and dosed with live M13(pBluescript II) (n = 3); (2) colonized with Sm^{R} W1655 F+ and dosed with heat-inactivated phage; (3) colonized with Sm^{R} W1655 F+ and dosed with live phage (n = 4). Colonized mice were treated with 10^{14} phage on Day 0 and carbenicillin was added to the water. CFU per gram feces (black) and percent Carb^{R} (red) were determined on MacConkey agar with antibiotic selection. **(d)** M13-based delivery of antibiotic resistance gene is phage dose-dependent. M13(pBluescript II) was ten-fold serially diluted from 10^{14} to 10^{7}. Mice (n = 24) were gavaged with a single dilution on Day 0 and carbenicillin was added to the water. On Day 2, Carb^{R} CFU per gram feces was determined on MacConkey agar with antibiotic selection. Sm, streptomycin; Amp, ampicillin; Carb, carbenicillin; dashed line, limit of detection for CFU per gram feces.

treatment (Figure 1b). When selection was lifted on Day 7, recolonization was observed for 5 of the 6 mice; when carbenicillin was again introduced on Day 13, colonization again dropped dramatically following dynamics similar to the first exposure. The very low background *E. coli* in the gut during carbenicillin treatment, as well as the lack of emergent spontaneous resistant cells able to recolonize during either the first or second antibiotic exposure, indicates that using a beta-lactam antibiotic in the drinking water is a very effective means of selection in our setup.

With an understanding of the dynamics of antibiotic selection *in vivo*, we next pursued the phage-mediated delivery of a resistance gene. Reports in the literature suggested that while M13 can withstand low pH [57], it may not fare so well in gastric juice [58]. We reasoned that we may be able to overcome this potential obstacle by relying on our selective power — that is, even if phage viability and frequency of infection events were low, the ability to apply selection for infected cells would give us an strong advantage for detection. To deliver a Carb^R gene to *E. coli* in the gut, we first generated M13 phage carrying pBluescript II using established methods for helper-mediated packaging of phagemid DNA. Next, we colonized mice with either Sm^R *E. coli* W1655 F+ (M13^S) or W1655 F− (M13^R as a control) and subsequently dosed them with either live phage or a heat-inactivated preparation of the same phage (Figure 1c). After dosing the mice with approximately 10^{14} M13 phage carrying Carb^R, we immediately transferred them to water containing carbenicillin, and then tracked both total *E. coli* and Carb^R *E. coli* in the feces for 7 days. Colonization levels fell rapidly and stayed near or below the limit of detection in control mice that were either colonized with F− and given live phage or colonized with F+ but given heat-inactivated phage; in contrast, when mice were colonized with F+ and dosed with live phage, there was only a transient drop in colonization on the first day, during which the rise of Carb^R cells occurred, and colonization was re-established within one day by an *E. coli* population that was resistant to carbenicillin (Figure 1c). These results show that orally dosed M13 phage were indeed able to infect *E. coli* in the GI tract and deliver a plasmid conferring resistance to carbenicillin.

We confirmed these results in an independent animal experiment in which mice were colonized by Sm^R *E. coli* W1655 F+ and orally dosed with ten-fold serial dilutions of phage carrying Carb^R, from 10^{14} phage down to 10^7 phage (n = 2 or 3 per dose). We found that colonization by Carb^R *E. coli* was consistent across high phage doses (10^{14} and 10^{13}) but variable at lower doses (10^{12} to 10^9), suggesting that factors other than number of phage introduced into the mouse can impact colonization outcome (Figure 1d). We confirmed that resistance to carbenicillin was indeed due to M13-mediated transfer of the plasmid pBluescript II by extracting plasmid DNA from fecal Carb^R *E. coli* isolates from the 11 mice that were successfully colonized; comparison of restriction-digested plasmid DNA to linearized pBluescript II confirmed that isolates from all 11 mice carried plasmid DNA of the expected size (Figure S3). These results show that plasmid DNA was indeed transferred from M13 phage particles into recipient *E. coli* colonizing the GI tract.

M13 carrying CRISPR-Cas9 can target *E. coli in vitro*

We next asked whether M13 could be used to deliver vectors that carry CRISPR-Cas9 for sequence-specific targeting of *E. coli*. We first generated two fluorescently marked isogenic derivatives of Sm^R W1655 F+ using the *mcherry* or the *sfgfp* marker gene, with the goal of using CRISPR-Cas9 to target the latter. We next constructed M13-compatible non-targeting (NT) and GFP-targeting (GFPT) CRISPR-Cas9 vectors by cloning the spacers sequences, *bla* gene, and f1 origin of replication into the previously described low-copy vector pCas9 [59], generating pCas9-NT-f1A/B and pCas9-GFPT-f1A/B (Figure S4). The *bla* and f1 *ori* were cloned as a fragment from pBluescript II in both possible orientations (A or B) to make possible M13 ssDNA packaging of either strand of vector DNA, a feature determined by the orientation of the f1 *ori*. We packaged these phagemids into M13 using a helper strain and called resulting phage NT M13 or GFPT M13. The phage were used to infect the GFP- or mCherry-marked strains and cells were diluted and spotted on solid media containing carbenicillin to select for the transferred phagemid. We found that GFP-marked *E. coli* infected with GFPT M13 exhibited impaired colony growth relative to the NT M13 control (Figure 2a and Figure S5). Interestingly, we did not observe a large decrease in the total number of CFUs indicating that despite impaired growth, M13-delivered CRISPR-Cas9 could be overcome by mechanisms enabling cell survival under targeting conditions.

Given that GFP-marked cells could withstand GFPT M13, we next focused on survivors to examine possible means of escaping CRISPR-Cas9. We subjected colonies arising from infection with NT M13 or GFPT M13 (Figure 2a) to streak purification and observed that of 16 clones from the GFPT set, 11 lost GFP fluorescence while 5 maintained fluorescence (Figure 2b). We isolated genomic DNA from these 16 clones, as well as 4 clones from the NT control, and used PCR to verify presence or absence of the *sfgfp* gene. As expected, all 4 NT clones as well as the 5 GFPT clones that retained GFP fluorescence possessed the *sfgfp* gene; analysis of the CRISPR-Cas9 phagemid revealed that of these latter 5 clones, 4 had lost the targeting spacer (Figure S6). In contrast, the 11 non-fluorescent clones retained the spacer (Figure S6) and appeared to have chromosomal deletions of or encompassing the target gene, with 10 being negative for a PCR product (Figure 2c) and 1 exhibiting a partial loss of the coding sequence that includes the site targeted by Cas9 under GFPT conditions (Figure S7). These data suggest that in most cases, escape from CRISPR-Cas9 by target site mutation is accompanied by gene loss and are consistent with previous work showing that chromosomal cleavage by Cas9 in *E. coli* can be repaired by homologous recombination leading to large deletions up to 35 kb [60].

Although it was possible for GFP-marked cells to overcome CRISPR-Cas9, we wanted to take advantage of the growth defect of cells under targeting conditions; that is, because GFP-marked *E. coli* showed impaired growth visible in colony morphology, we next asked if GFPT M13 infection of a co-culture of GFP-marked and mCherry-marked strains would lead to the the former being

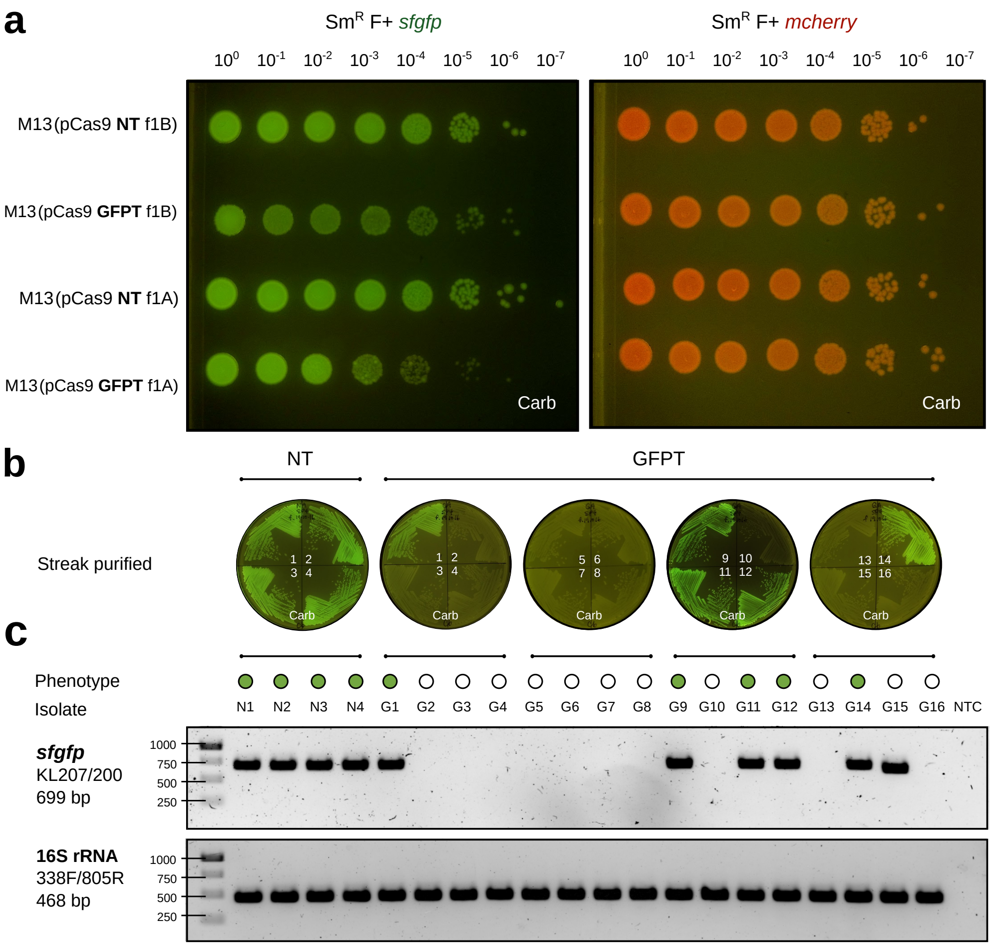

Figure 2. M13-mediated delivery of CRISPR-Cas9 to *E. coli* cells *in vitro* causes impaired colony growth and can induce chromosomal deletions that encompass the targeted gene. (a) GFP-marked *E. coli* exhibit a sick colony morphology after infection with M13 phage carrying GFP-targeting CRISPR-Cas9. M13 phage with non-targeting (NT) or GFP-targeting (GFPT) CRISPR-Cas9 were used to infect Sm^R F+ GFP-marked *E. coli* or mCherry-marked *E. coli* as a negative control. Cells were incubated with phage for infection then serially diluted and spotted onto media with selection for the CRISPR-Cas9 vector. Designation of f1A or f1B indicates the DNA strand of the vector in M13 phage, dependent on the orientation in which the f1-*bla* fragment was cloned. **(b)** CRISPR-Cas9 targeting the GFP gene can induce loss of fluorescence. Colonies arising from infection with M13 phage carrying either NT or GFPT CRISPR-Cas9 were subjected to several rounds of streak purification on selective media to ensure phenotypic homogeneity and clonality. The majority (11/16) of GFP-targeted streak purified clones lost GFP fluorescence. **(c)** Clones exhibiting a loss of fluorescence due to GFPT CRISPR-Cas9 have chromosomal deletions of or encompassing the targeted gene. Genomic DNA was isolated from streak-purified clones and PCR was used to determine whether the GFP gene was present; PCR for the 16S rRNA gene was performed as a positive control.

outcompeted. We started co-cultures of the two strains, adding either NT M13 or GFPT M13 followed by carbenicillin to select for phage infection of cells; we sampled the co-cultures every 4 h over a period of 24 h by washing, diluting, and spotting cells onto non-selective solid media to assess the relative abundance of the two strains. We found that GFPT M13 led to fewer GFP-fluorescent colonies at 4 h and onwards, relative to the NT M13 control (Figure 3a). However, we observed that at the later timepoints (16, 20, and 24 h), healthy GFP fluorescent colonies arose at dilutions in which they were growth-impaired at earlier timepoints. We asked whether unimpaired growth of the GFP-marked strain at these later timepoints could be due to enzymatic inactivation of carbenicillin in the culture thereby relaxing the selection for the phagemid over time. We tested the supernatant for carbenicillin using a bioassay with the indicator organism *Bacillus subtilis* 168 and found that the vast majority of the antibiotic was not detected in cultures after 4 h whereas it was detected at all timepoints in the sterile control (Figure 3b); furthermore, these GFP fluorescent colonies were largely absent when the same co-culture was spotted onto media containing carbenicillin (Figure S8), indicating that the recovery of GFP+ cells at later timepoints in the co-culture could be due to lack of selection leading to loss of the phagemid carrying GFPT CRISPR-Cas9.

To more quantitatively assess the abundance of the two fluorescent strains in competition after infecting with NT or GFPT M13 phage, we turned to flow cytometry. We repeated the co-culturing experiment in triplicate and quantified GFP+ and mCherry+ events 8 h after adding phage and carbenicillin to select for phage infection. Compared to the NT control, the co-culture infected with GFPT M13 exhibited both fewer GFP+ events (34% versus 62% for NT control; Figure 3c) as well as a shift in the distribution of GFP+ events towards lower fluorescence leading to a bimodal distribution (peak intensities of 44654 and 8943 versus a single peak of 31441 for the NT control; Figure 3d). Interestingly, the relative abundance of GFP+ was higher than would be expected from

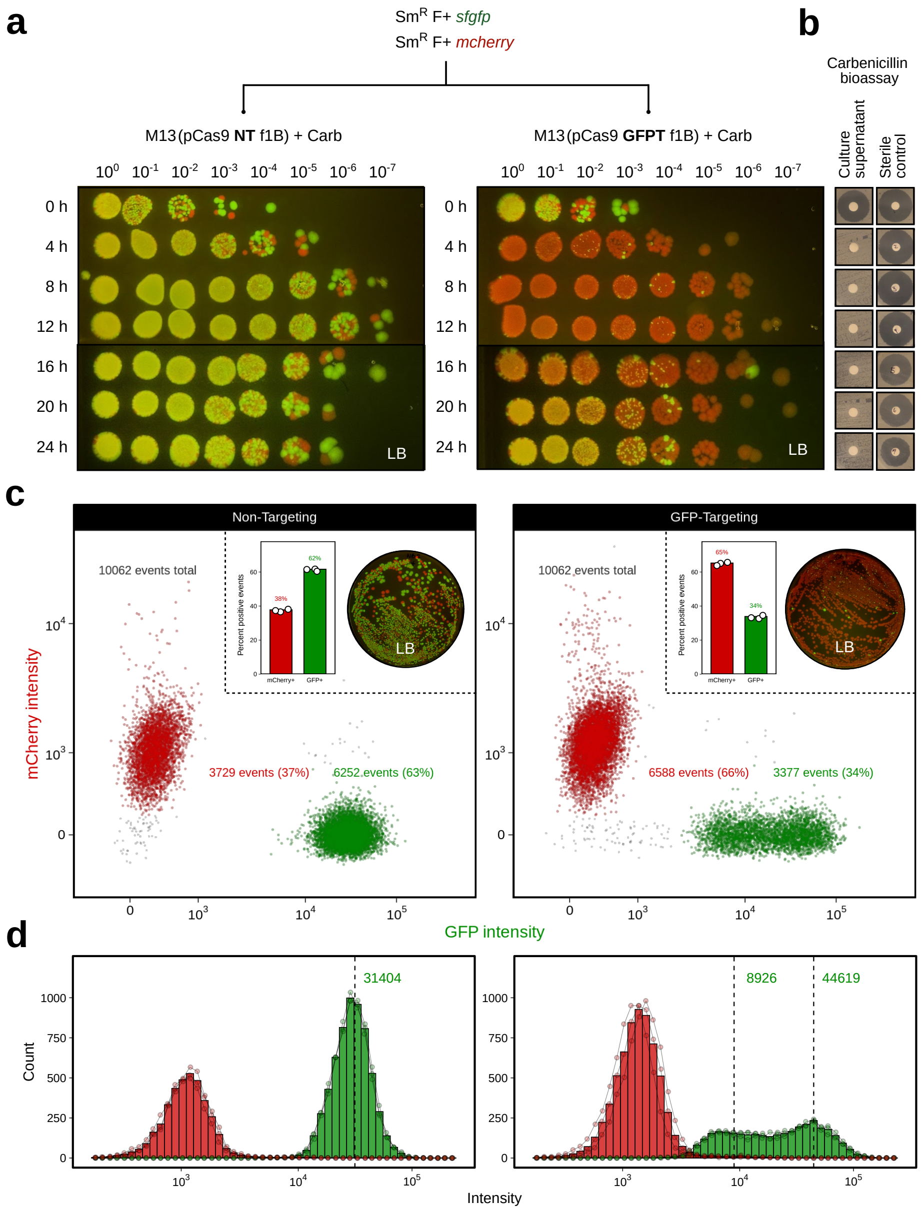

Figure 3. M13-delivered CRISPR-Cas9 for sequence-specific targeting of *E. coli* in *in vitro* co-cultures of fluorescently marked isogenic strains. (a) M13-delivered GFPT CRISPR-Cas9 leads to reduced competitive fitness of the GFP-marked strain. A co-culture of Sm^R F+ *sfgfp* and Sm^R F+ *mcherry* was incubated with M13 phage carrying non-targeting (NT) or GFP-targeting (GFPT) CRISPR-Cas9 at a starting MOI of approximately 500. Carbenicillin was added to a final concentration of 100 µg/µl to select for phage infection. Co-cultures were sampled every 4 hours over 24 hours; cells were washed, serially diluted, and spotted onto non-selective media to assess targeting of the GFP-marked strain. **(b)** Carbenicillin in culture supernatants was not detectable within 4 hours of growth, using a carbenicillin bioassay against indicator strain *Bacillus subtilis* 168; bioassay detection limit approximately 2.5 µg/µl. **(c)** Flow cytometry of co-cultures 8 hours following the addition of phage and carbenicillin show reduced GFP+ events in the GFPT versus NT condition. Flow plot shows data from one of three replicates. Inset: bar graph quantifying percent GFP+ and mCherry+ events for three replicates (left); plating results for a single replicate on non-selective media (right). **(d)** GFPT CRISPR-Cas9 changes the shape of the distribution of GFP+ population. Histogram of mCherry+ and GFP+ events by intensity shows that a proportion of GFP+ cells in the GFPT condition have shifted to a state of lower fluorescence. Bars indicate mean of three replicates; connected points are individual replicates.

plating results of the same co-cultures at 8 h (Figure 3c inset), indicating that GFP+ cells may be able to survive in liquid media under targeting conditions but be unable to form colonies on solid media. To confirm these results, we repeated flow cytometry on the co-cultures at 8 h and 24 h, finding that GFP+ events further decreased at 24 h in the GFPT condition (17% versus 63% for NT; Figure S9). Although there was a discrepancy between the flow cytometry and the plating results likely due to differences in survival in liquid versus on solid media, both methods demonstrated that M13 phage delivering GFP-targeting CRISPR-Cas9 can impair the GFP-marked strain. Given these results *in vitro*, we next wanted to determine if GFPT M13 could be used to selectively target *E. coli in vivo*.

Sequence-specific depletion of *E. coli in vivo* using M13-delivered CRISPR-Cas9

Because the mCherry-marked strain could outcompete the GFP-marked strain under targeting conditions with GFPT M13, we next asked whether this was also true *in vivo*. To answer this question, we returned to the streptomycin-treated mouse model. We introduced both $\mathrm{Sm^R}$ F+ *sfgfp* and $\mathrm{Sm^R}$ F+ *mcherry* strains into mice, then orally dosed them with either 10^{11} NT M13 or GFPT M13 and added carbenicillin in the water to select for phage infection; after one week of carbenicillin treatment, we removed it from the water and followed mice for an additional week to determine whether phage-induced changes would persist in the absence of maintaining selection (Figure 4a). We collected and assayed fecal samples using flow cytometry from 5 different timepoints: Day -3, before introduction of fluorescent *E. coli* strains; Day 0, at which both strains are present; Day 2, after phage and carbenicillin have been applied; Day 7, after one week of carbenicillin treatment; and Day 14, one week after carbenicillin was removed (Figure 4b shows example time series flow cytometry data for one mouse from each of the NT and GFPT group; all data are shown in Figure S10).

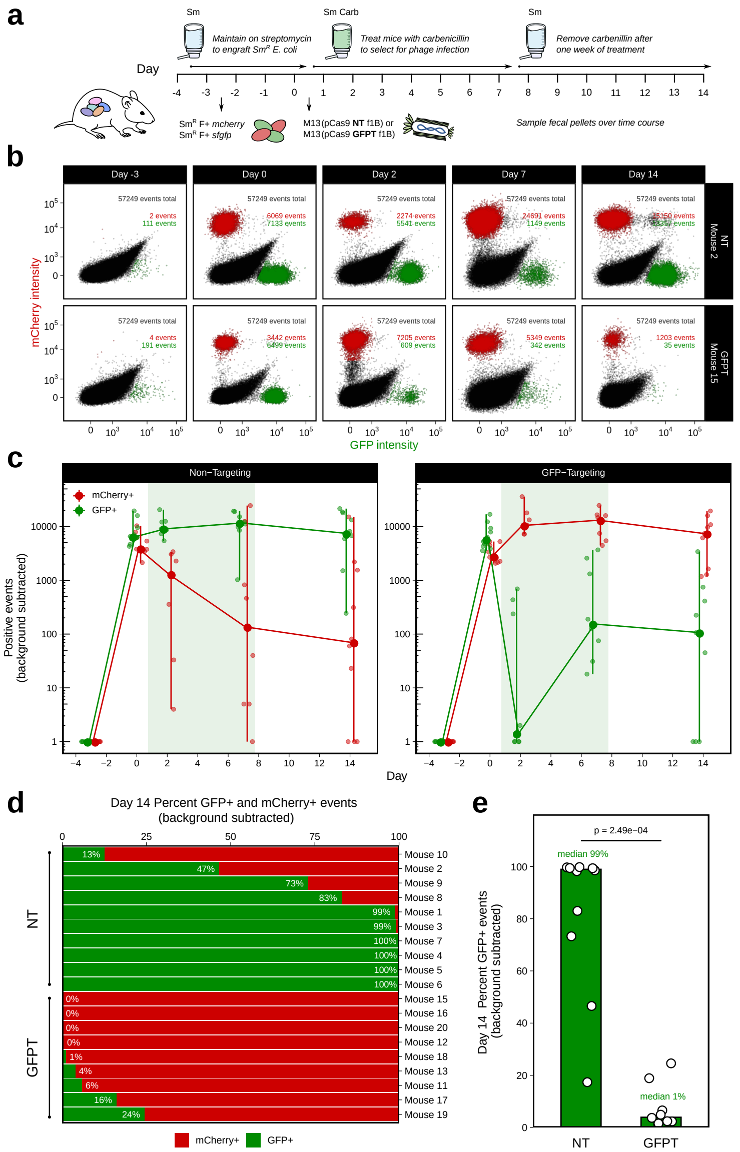

Figure 4. M13-delivered CRISPR-Cas9 for sequence-specific depletion of *E. coli* in the gut of mice colonized by competing fluorescently marked isogenic strains. (a) Experimental timeline: Day -3, mice were colonized with an approximately 50/50 mixture of Sm^R F+ *sfgfp* and *mcherry* using the streptomycin treatment model; Day 0, mice were dosed with 10^{11} M13 phage carrying non-targeting (NT) or GFP-targeting (GFPT) CRISPR-Cas9 ($n = 10$ per group) and carbenicillin was added to the drinking water; Day 7, carbenicillin was removed from the drinking water; Day 14, experimental endpoint. Fecal samples were collected throughout for analysis. **(b)** M13-delivered GFPT CRISPR-Cas9 can lead to loss of the GFP-marked strain. Time series flow plots of fecal samples for select mice, one from each of the NT and GFPT groups. Top right: total number of events as well as number of red and green events. **(c)** Mice in the GFP-targeting group exhibited a decrease in the number of GFP+ events in fecal samples over time compared to the non-targeting control group. For each mouse, GFP+ and mCherry+ events from Day -3 (before introduction of *E. coli*) were used to subtract background at all subsequent timepoints; timepoints were excluded in which both the GFP+ and the mCherry+ events were below a background threshold of maximum background observed for that fluorophore multiplied by a factor of three. Line graph: points indicate median; vertical lines indicate range of values observed. **(d)** Mice in the GFPT group exhibited depletion and even loss of the GFP-marked strain. Percent GFP+ and mCherry+ events for each mouse on Day 14. Mice were excluded if both the GFP+ and mCherry+ events were both below their respective background thresholds. **(e)** A significant difference was observed in the distribution of mice in the GFPT group versus NT control with respect to GFP+ events in fecal samples at Day 14. Bars are medians; p-value, Mann-Whitney test. Sm, streptomycin; Carb, carbenicillin.

For each mouse, we tracked GFP+ and mCherry+ events, using data from Day -3 (prior to *E. coli*) to subtract background positive events for both fluorophores, on a per mouse basis. We found that on average, while the GFP-marked strain appeared to fair better *in vivo* than the mCherry strain under NT conditions, GFP+ events under GFPT conditions exhibited a sharp decrease on Day 2, with some mice exhibiting levels at or near background; this was followed by a slight recovery on Days 7 and 14 but to levels markedly below those in the NT control (Figure 4c; individual mouse data are shown in Figure S11). We confirmed the large decrease in GFP+ events on Day 2 by culturing from mouse fecal samples, finding that culturing results were consistent with flow cytometry data (Figure S12).

At the final timepoint, 14 days after receiving phage, the relative abundance of GFP+ events in the fecal samples of mice in the GFPT group was significantly different than the NT group ($p = 2.5e{-4}$, Mann-Whitney test); furthermore, in 4 mice that received GFPT M13, the GFP-marked strain was successfully outcompeted by the mCherry strain and GFP+ events were not detected above background levels, an outcome that was not observed for any mouse in the NT condition (Figure 4d and e). In fact, for mice receiving NT M13, the opposite tended to be true: we observed that the relative abundance of GFP+ events was much higher on average than mCherry+ events (median 99% GFP+ for NT). These *in vivo* competition data indicate that it is possible to use M13 phage carrying CRISPR-Cas9 for sequence-specific depletion of an otherwise isogenic bacterial strain in the mouse gut.

M13-delivered CRISPR-Cas9 can induce chromosomal deletions *in vivo*

With positive results for strain-specific targeting using CRISPR-Cas9 against one of two strains both *in vitro* and *in vivo*, we next returned to the idea of using GFPT M13 against only a single strain of *E. coli* in the gut. That is, would it be possible to select for cells that have escaped CRISPR-Cas9 targeting through genomic deletion events *in vivo*, as was observed *in vitro*

(Figure 2c)? To answer this question, we first constructed a double-marked Sm^R F+ *sfgfp mcherry* strain so that we could use flow cytometry to visualize loss of GFP fluorescence in mouse fecal samples, reasoning that double-positive events would shift to singly mCherry-positive events if the targeted *sfgfp* gene were to be lost. Following a similar regimen as the *in vivo* competition experiment (Figure 4a), we introduced the double-marked GFP+ mCherry+ strain into mice, then orally dosed them with either 10^{11} NT M13 or GFPT M13 and added carbenicillin in the water; after one week, we removed carbenicillin and followed mice for another week (Figure 5a).

Again, we collected and assayed fecal samples using flow cytometry from 5 different timepoints: Day -5, before introduction of fluorescent *E. coli*; Day 0, when the strain is present; Day 2, after phage and carbenicillin have been applied; Day 7, after one week of carbenicillin treatment; and Day 14, one week after carbenicillin was removed. For each mouse, we used fluorescence levels on Day -5 (pre-*E. coli*) to account for background GFP+ mCherry+ events and those on Day 0 (pre-phage) to account for background mCherry+ events. After phage treatment, we observed the emergence of singly positive mCherry+ events in a subset of the mice given GFPT M13, an outcome that was not observed for the NT control, indicating cells had lost GFP fluorescence *in vivo* (Figure 5b shows example time series flow cytometry data for one mouse from each of the NT and GFPT group; all data are shown in Figure S13).

We tracked fluorescent events over time (Figure S14a) and found that by the final timepoint, mCherry+ events were detected in the fecal samples of 3 of 8 mice that remained positive for either singly or doubly positive events over background, with the relative abundance of the mCherry+ population being highly variable at 12%, 49%, and 96% (Figure 5c). We confirmed these outcomes by culturing from GFPT mouse fecal samples on Day 14, finding presence of red fluorescent colonies in proportions consistent with flow cytometry results (Figure 5d and Figure S14b). These data indicate that while it is possible for CRISPR-Cas9-induced genomic deletion events to occur *in*

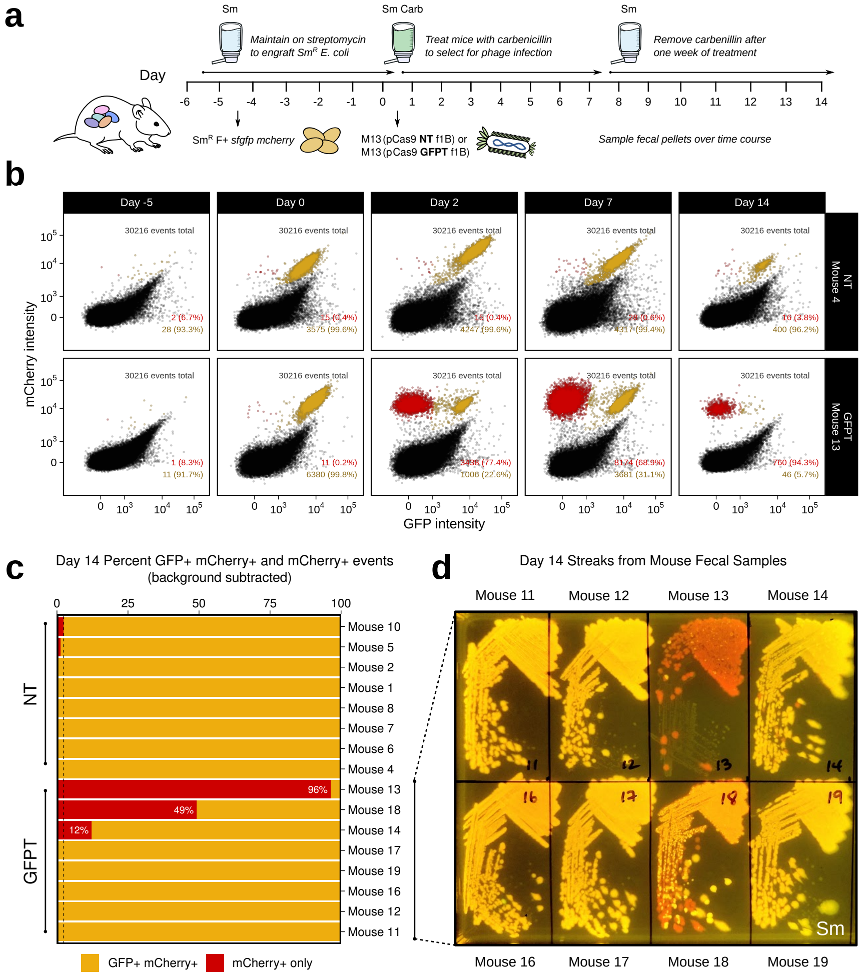

Figure 5. M13-delivered CRISPR-Cas9 can induce chromosomal deletions encompassing the targeted gene in *E. coli* colonizing the mouse gut. (a) Experimental timeline: Day -5, mice were colonized with double-marked Sm^R F+ *sfgfp mcherry* using the streptomycin treatment model; Day 0, mice were dosed with 10^{11} M13 phage carrying non-targeting (NT) or GFP-targeting (GFPT) CRISPR-Cas9 (n = 10 per group) and carbenicillin was added to the drinking water; Day 7, carbenicillin was removed from the drinking water; Day 14, experimental endpoint. Fecal samples were collected throughout for analysis. **(b)** M13-delivered GFPT CRISPR-Cas9 can cause loss of GFP fluorescence in double-marked *E. coli*. Time series flow plots of fecal samples for select mice, one from each of the NT and GFPT groups. Top right: total number of events; bottom right: singly mCherry+ events and doubly GFP+ mCherry+ events. **(c)** Fecal samples of three of eight mice in the GFPT group were positive for mCherry-only fluorescence on Day 14. Percent GFP+ mCherry+ and mCherry+ only events for each mouse. Mice were excluded if both populations were below a background threshold of maximum background observed for that population multiplied by a factor of three. Dashed line indicates maximum mCherry fluorescence observed for the NT group. **(d)** Culture of *E. coli* from fecal samples of the GFPT group on Day 14 confirmed loss of GFP leading to red rather than dual fluorescence. Colonies exhibiting only red fluorescence were observed for Mouse 13, 14, and 18 in proportions consistent with flow cytometry results. Sm, streptomycin; Carb, carbenicillin.

vivo, resultant deletion strains may or may not outcompete the parent strain. Furthermore, 5 of 8 mice in the GFPT group remained colonized by only the double-marked strain, suggesting that escape from CRISPR-Cas9 targeting through chromosomal deletion events may be a more improbable outcome than escape via mutations that inactivate the CRISPR-Cas9 system. Because spacer loss via plasmid recombination is a common mode of escape, we isolated singly (red) and doubly (yellow) fluorescent *E. coli* from feces of mice on Day 2 and extracted plasmid DNA to ask whether phagemids still carried the expected spacer. All fluorescent yellow isolates from NT mice had the expected spacer, as well as all fluorescent red isolates from GFPT mice; however, phagemid DNA isolated from fluorescent yellow isolates from the GFPT mice had all undergone recombination events, with 4 of 5 confirmed to have recombined only within the CRISPR array leading to loss of the spacer targeting the *sfgfp* gene (Figure S15).

Discussion

In this work, we use phage M13 and its host *E. coli* to demonstrate that bacterial viruses can be used for gene delivery to bacterial cells that are colonizing the gut. Specifically, in a series of highly controlled experiments using a standard phagemid vector, we show that M13 can infect and transfer the vector to *E. coli* engrafted in the gut of mice. We then construct phagemid vectors carrying CRISPR-Cas9 and use M13 as chassis to deliver these constructs to *E. coli*. Using strain competition in the gut, we first show that CRISPR-Cas9 targeting is sequence-specific and able to selectively decrease the abundance of the targeted strain. Second, in the absence of competition with a non-targeted strain, we show that M13-delivered CRISPR-Cas9 can generate loss of the target gene *in vivo* through homologous recombination, indicating that CRISPR-Cas9 can be employed to remove genes from bacteria while still enabling cell survival.

Development of CRISPR-Cas9 to target bacteria in the gut requires careful consideration of the mechanisms by which cells may escape killing. Although the use of M13-delivered CRISPR-Cas9 as an antimicrobial has been proposed [23], bacterial cells have been shown to be able to survive Cas9-induced double-stranded breaks by homologous recombination or non-homologous end-joining mechanisms [60]. In particular, RecA-mediated homology-directed repair is a highly conserved and robust response wherein induced cells may find a repair template sharing homology within minutes [61]. That targeted strains can readily escape killing suggests that rather than being used as an antimicrobial in the gut, phage-delivered CRISPR-Cas9 may instead be well suited for gut microbiome editing in the form of targeted genomic deletions, leveraging the conserved DNA repair pathways present in bacteria. One advantage of this approach is that specific genes could be targeted for removal from the gut microbiome whilst the community as a whole remains more intact than if the organism were to be removed entirely. This idea is consistent with previous use of CRISPR-Cas9 to target plasmid rather than chromosomal DNA [23, 24, 62]. An alternative to Cas9 would be to use CRISPR-Cas3 systems in which the larger DNA lesions may be more difficult to repair [63], although spacer loss leading to escape by *C. difficile* in the mouse gut has also been reported [26]. Likely irrespective of the particular system chosen for deployment *in vivo*, gut microbiome editing will require iterative improvements on the design of delivered CRISPR-Cas constructs to try to mitigate mutations that render the system inactive, or to decrease the probability of these events relative to either killing or gene loss events, the probability of which may also be locus-dependent.

Here, we demonstrate that filamentous phage can be used to deliver genetic cargo to bacterial cells in the mouse gut using CRISPR-Cas9 as proof-of-concept, but there are many potential applications for gene delivery to commensal bacteria. Furthermore, although we use phage in combination with an antibiotic treatment, alternative (i.e., non-antibiotic) strategies to select for or enrich for cells that have been infected in the gut would be immensely useful to minimize large disruptions to the existing gut microbiota. Issues including phage survival, phage infection frequency, and selection for cells that have been infected by phage may be influenced by the choice of phage chassis, target bacterium, and cargo design. These factors will have to be well understood if the potential of phage-based gene delivery to the microbiota is to be fully realized. Foundational, reductionist, and highly controlled studies such as ours will be valuable not only to establish *in vivo* models with which to study specific phage-bacteria interactions but also to assess the feasibility, utility, and possible limitations of phage-based gene delivery, particularly as the microbiome research community aspires to the genetic manipulation of diverse bacterial members of the gut microbiota and turns to phage as potential tools for *in vivo* microbiome editing.

Acknowledgments

We thank Jessie Turnbaugh, Kimberly Ly, Jolie Ma, and staff at the UCSF animal facility for animal care and assistance with learning animal procedures. We are grateful to Daryll Gempis, Bernarda Lopez, and Ernesto Valencia of the UCSF G.W. Hooper Foundation for laboratory and administrative support. We thank Katja Engel (University of Waterloo) for help in translating the original publication on the isolation of M13 written in German. We are grateful to Antoine Vigouroux (Institut Pasteur) for generously sharing MG1655 derivatives carrying *sfgfp* and *mcherry* marker genes. We thank the Chan-Zuckerberg BioHub for sequencing through the Microbiome Initiative. We are grateful to Joseph Bondy-Denomy and Oren Rosenberg (UCSF) for constructive criticism on the manuscript. The graphic of a laboratory mouse was adapted from a Wikimedia Commons graphic distributed under CC-BY-SA-4.0 by Gwilz.

Author Contributions

KNL and PJT conceived the ideas. KNL supervised laboratory work and analyzed the data. KNL, PS, PSP, and PJT designed the experiments. KNL and PS constructed *E. coli* strains. KNL and PSP constructed plasmids. KNL performed phage and animal experiments with assistance from PSP. PS and KNL performed antibiotic assays. KNL, FBY, and JEB performed 16S rRNA gene sequencing with assistance from PSP and MN. MA performed flow cytometry with assistance from KNL. KNL analyzed mouse fecal isolates with assistance from MN. PJT provided reagents and materials. KNL made the figures and drafted the manuscript; PJT, PS, PSP, MA, JEB, and FBY assisted with editing.

Funding

KNL and PS were both supported by a postdoctoral fellowship from the Canadian Institutes of Health Research (CIHR), JEB by a postdoctoral fellowship from the Natural Sciences and Engineering Research Council of Canada (NSERC), MA by an F32 fellowship from the National Institutes of Health (F32AI147456-01), and PSP by a scholarship from the UCSF Discovery Fellows Program. This work was supported by the National Institutes of Health (PJT, R01HL122593). PJT holds an Investigators in the Pathogenesis of Infectious Disease Award from the Burroughs Wellcome Fund, is a Chan Zuckerberg Biohub investigator, and was a Nadia's Gift Foundation Innovator supported, in part, by the Damon Runyon Cancer Research Foundation (DRR-42-16) and the Searle Scholars Program (SSP-2016-1352).

Conflict of Interest Statement

KNL, PS, and PJT are listed inventors on a U.S. provisional patent application related to this work (33167/55262P1). PJT is on the scientific advisory boards for Kaleido, Pendulum, Seres, and SNIPRbiome. All other authors declare no competing interests.

Methods

Bacterial strains, plasmids, phage, and oligonucleotides. Strains, plasmids, and phage used in this study, including description and sources, are provided in Table 1. Oligonucleotides used in this study are provided in Table 2.

Table 1. Bacterial strains, plasmids, and phage.

Resource	Relevant Characteristics	Ref./Source
Strain		
XL1-Blue MRF'	Phage propagation with helper M13KO7; Tc^R	Agilent
DH5alpha	Routine cloning; phage propagation with helper HP4_M13	[64]
MG1655	Derivative of K-12	[65]
W1655 F−	Derivative of K-12; $M13^R$	ATCC 23737
W1655 F+	Derivative of K-12; $M13^S$	ATCC 23590
MG1655 *rpsL*-Sm^R	Spontaneous *rpsL*-Sm^R (Lys42Arg) derivative of MG1655	This study
W1655 F− *rpsL*-Sm^R	Recombineered *rpsL*-Sm^R (Lys42Arg) derivative of W1655 F−	This study
W1655 F+ *rpsL*-Sm^R	Recombineered *rpsL*-Sm^R (Lys42Arg) derivative of W1655 F+	This study
AV01::pAV01	MG1655 with constitutive *sfgfp* clonetegrated at HK022 *att* site; Km^R	[66]
AV01::pAV02	MG1655 with constitutive *mcherry* clonetegrated at lambda *att* site; Km^R	[66]
W1655 F+ *rpsL*-Sm^R *sfgfp*	Sm^R W1655 F+ with *sfgfp* transduced from AV01::pAV01; Km^S	This study
W1655 F+ *rpsL*-Sm^R *mcherry*	Sm^R W1655 F+ with *mcherry* transduced from AV01::pAV02; Km^S	This study
W1655 F+ *rpsL*-Sm^R *sfgfp mcherry*	Sm^R W1655 F+ *sfgfp* with *mcherry* transduced from AV01::pAV02; Km^S	This study
Plasmid		
pBluescript II KS(-)	Commercial phagemid; $Carb^R$	Agilent
pSIJ8	Temperature-sensitive; lambda Red recombineering; $Carb^R$	[67]
pE-FLP	Temperature sensitive; constitutive flippase expression; $Carb^R$	[68]
pCas9	Low-copy vector carrying *cas9*, tracrRNA, and CRISPR array; Cm^R	[59]
pCas9-NT-f1A	pCas9 with non-targeting spacer; f1-*bla* in orientation A; Cm^R $Carb^R$	This study
pCas9-NT-f1B	pCas9 with non-targeting spacer; f1-*bla* in orientation B; Cm^R $Carb^R$	This study
pCas9-GFPT-f1A	pCas9 with GFP-targeting spacer; f1-*bla* in orientation A; Cm^R $Carb^R$	This study
pCas9-GFPT-f1B	pCas9 with GFP-targeting spacer; f1-*bla* in orientation B; Cm^R $Carb^R$	This study
Phage / Helper		
M13KO7	Helper phage; Km^R	NEB
HP4_M13	Helper plasmid; Km^R	[69]
P1	Transducing phage	ATCC 25404-B1

Table 2. Oligonucleotides used in this study.

Oligo ID	Oligo Sequence 5'–3'	Purpose
PS-rpsL1	`CGTGGCATGGAAATACTCCG`	F primer to amplify *rpsL* for recombineering
PS-rpsL2	`GCATCGCCCTAAAATTCGGC`	R primer to amplify *rpsL* for recombineering
PSP116	`AAACCCTTCACCTTCACCACGAACAGAGAATTTG`	Oligo 1 to generate GFPT spacer
PSP117	`AAAACAAATTCTCTGTTCGTGGTGAAGGTGAAGG`	Oligo 2 to generate GFPT spacer
PSP120	`AAACATCGCACATCCTGGTCGCGACATTAAGAGT`	Oligo 1 to generate NT spacer
PSP121	`AAAAACTCTTAATGTCGCGACCAGGATGTGCGAT`	Oligo 2 to generate NT spacer
PSP108	`TTAATAAATGCAGTAATACAGG`	Primer to sequence spacer in CRISPR array
KL215	`CCTGTCGACGGTATCGATAAGCTTGATATCG`	F primer to clone f1-*bla* from pBluescript II as SalI fragment
KL216	`CCTGTCGACGATTATCAAAAAGGATCTTCACCTAGATCC`	R primer to clone f1-*bla* from pBluescript II as SalI fragment
KL207	`CTGTTCACCGGTGTTGTTCC`	F primer to amplify *sfgfp* fragment
KL200	`TTATTTGTAGAGTTCATCCATGCCG`	R primer to amplify *sfgfp* fragment
BAC338F	`ACTCCTACGGGAGGCAG`	F primer to amplify 16S rRNA gene fragment
BAC805R	`GACTACCAGGGTATCTAATCC`	R primer to amplify 16S rRNA gene fragment
V4 515F Nextera	`TCGTCGGCAGCGTCAGATGTGTATAAGAGACAGGTGCCAGCMGCCGCGGTAA`	F primer for 16S rRNA gene sequencing primary PCR
V4 806R Nextera	`GTCTCGTGGGCTCGGAGATGTGTATAAGAGACAGGGACTACHVGGGTWTCTAAT`	R primer for 16S rRNA gene sequencing primary PCR
Various (Table S1)	`AATGATACGGCGACCACCGAGATCTACACNNNNNNNNTCGTCGGCAGCGTC`	F primer for 16S rRNA gene sequencing indexing PCR
Various (Table S1)	`CAAGCAGAAGACGGCATACGAGATNNNNNNNNGTCTCGTGGGCTCGG`	R primer for 16S rRNA gene sequencing indexing PCR

Minimum inhibitory concentration (MIC) assay. Cells were prepared by standardizing an overnight culture to an OD_{600} of 0.1 using saline, and further diluted ten-fold in saline then ten-fold in LB. The drug was prepared by dissolving antibiotic in vehicle (sterile distilled water) and filter-sterilizing, then serially diluting two-fold in vehicle to prepare 100× stock solutions, and finally diluting ten-fold in LB for 10× stock. To wells of a 96-well plate, 60 µl of LB, 15 µl of drug, and 75 µl of cells were added and mixed well. Final drug concentrations ranged between 0.002 µg/ml to 1000 µg/ml for ampicillin and 0.24 µg/ml to 2000 µg/ml for carbenicillin. The plate was incubated overnight at 37 °C without shaking and OD_{600} was measured the following morning after agitation.

16S rRNA gene sequencing. Mouse fecal pellets were stored at –80 °C, DNA was extracted from single pellets using a ZymoBIOMICS 96 MagBead DNA Kit, and 16S rRNA gene sequencing was performed using a dual indexing strategy [70]. Briefly, primary PCR was performed using KAPA

HiFi Hot Start DNA polymerase (KAPA KK2502) and V4 515F/806R Nextera primers (Table 1). The reaction was diluted in UltraPure DNase/RNase-free water (Life Tech 0977-023) and used as template for a secondary (indexing) PCR using sample-specific dual indexing primers (Table 2 and Table S1). The reactions were normalized using a SequelPrep Normalization plate (Life Tech A10510-01) and the DNA was eluted and pooled. To purify and concentrate the DNA, 5 volumes of PB Buffer (Qiagen 28004) was added, mixed thoroughly, and purified using a QIAquick PCR Purification Kit (Qiagen 28106). The DNA was gel extracted using a MinElute Gel Extraction Kit (Qiagen 28604), quantified by qPCR using a KAPA Library Quantification Kit for Illumina Platforms (KAPA KK4824), and paired-end sequenced on the Illumina MiSeq platform. Data were processed using a 16S rRNA gene analysis pipeline [71] based on QIIME2 [72] incorporating DADA2 [73], and analyzed using R packages *qiime2R* v0.99.23 [74], *phyloseq* v1.33.0 [75], and *phylosmith* v1.0.4 [76]. Sample metadata are provided (Table S2) and raw sequence data have been deposited at the NCBI Sequence Read Archive under BioProject PRJNA642411 with accession numbers 12118792 to 12118959.

Construction of streptomycin-resistant *E. coli* strains. Strains resistant to the antibiotic streptomycin were generated by either selection for spontaneous resistance or by lambda Red recombineering [67, 77]. Spontaneous resistant mutants were selected by plating overnight cultures on LB supplemented with 500 µg/ml streptomycin. Lambda Red recombineering was later used to introduce a specific allele for genetic consistency between strains as different mutations in the *rpsL* gene can confer resistance to streptomycin [78]. Briefly, cells were transformed with the Carb^R temperature-sensitive plasmid pSIJ8 [67], and electrocompetent cells were prepared from cells grown in LB carbenicillin at 30 °C to early exponential phase and lambda Red recombinase genes were induced by addition of L-arabinose to 7.5 mM. Cells were electroporated with an *rpsL*-Sm^R PCR product amplified from a spontaneous streptomycin-resistant mutant of MG1655 using primers PS-rpsL1 and PS-rpsL2, and recombinants were selected on LB supplemented with 500 µg/ml streptomycin. The pSIJ8 plasmid was cured by culturing in liquid at 37 °C in the absence of carbencillin, plating for single colonies, and confirming Carb^S. The *rpsL* gene of Sm^R strains were confirmed by Sanger sequencing (Figure S16).

Construction of fluorescently marked *E. coli* strains. P1 lysates were generated of AV01::pAV01 and AV01::pAV02 carrying clonetegrated *sfgfp* and *mcherry*, respectively [66]. Briefly, 150 µl of overnight culture in LB supplemented with 12.5 µg/ml kanamycin was mixed with 1 µl to 25 µl P1 phage (initially propagated from ATCC on MG1655). The mixture was incubated for 10 minutes at 30 °C to aid adsorption, added to 4 ml LB 0.7% agar, and overlaid on pre-warmed LB agar supplemented with 25 µg/ml kanamycin 10 mM $MgSO_4$. Plates were incubated overnight at 30 °C, and phage were harvested by adding 5 ml SM buffer, incubating at room temperature for 10 minutes, and breaking and scraping off the top agar into a conical tube. Phage suspensions were centrifuged to pellet agar; the supernatant was passed through a 100 µm cell strainer, then through a 0.45 µm syringe filter, and lysates were stored at 4 °C. For transduction, 1-2 ml of recipient overnight culture was pelleted and resuspended in 1/3 volume LB 10 mM $MgSO_4$ 5 mM $CaCl_2$. 100 µl of cells was mixed with 1 µl to 10 µl P1 lysate and incubated at 30 °C for 60 minutes. To minimize secondary infections, 200 µl 1 M sodium citrate was added, followed by 1 ml of LB. The mixture was incubated at 30 °C for 2 h, then plated on LB 10 mM sodium citrate 25 µg/ml kanamycin to select for transductants. For excision of the vector backbone including the kanamycin resistance gene and heat-inducible integrase, cells were electroporated with pE-FLP [68]; transformants were selected on carbenicillin and confirmed for Km^S. pE-FLP was cured by culturing in liquid at 37 °C in the absence of carbencillin, plating for single colonies, and confirming Carb^S. Strains were subsequently grown routinely at 37 °C. For imaging fluorescent strains on agar, plates were typically incubated at 37 °C overnight, transferred to room temperature to allow fluorescence intensity to increase, and then imaged.

Engrafting *E. coli* in mice and preparation of antibiotic drinking water. Animal procedures were approved by the UCSF Institutional Animal Care and Use Committee. Specific pathogen free female BALB/c mice from the vendor Taconic were used for all mouse experiments. Streptomycin water was prepared by dissolving USP grade streptomycin sulfate (VWR 0382) in autoclaved tap water to a final concentration of 5 mg/ml and passing through 0.45 µm filtration units. Mice were provided streptomycin water for 1 day, followed by oral gavage of 0.2 ml containing approximately 10^9 CFU streptomycin-resistant *E. coli*. Mice were kept on streptomycin water thereafter to maintain colonization. For selection with beta-lactam antibiotics, USP grade ampicillin sodium salt (Teknova A9510) or USP grade carbenicillin disodium salt (Teknova C2110) was also dissolved in the water to a final concentration of 1 mg/ml. Drinking water containing streptomycin was prepared fresh weekly; with the addition of a beta lactam antibiotic, it was prepared fresh every 3-4 days.

Enumeration and culture of *E. coli* from mouse feces. Fecal pellets were collected from individual mice and CFU counts were performed on the same day. CFU per gram of feces was estimated by weighing the fecal pellet (typically 10-40 mg) on an analytical balance and suspending in 250 µl to 500 µl PBS or saline by manual mixing and vigorous vortexing. Large particulate matter was pelleted by centrifuging at $100\times g$, ten-fold serial dilutions were made in PBS, and 5 µl of each dilution was spotted on Difco MacConkey agar (BD 212123) supplemented with the appropriate antibiotics, i.e., streptomycin (100 µg/ml) or carbenicillin (50 µg/ml). For qualitative assessment of the fluorescent strains in feces, samples were spotted onto LB supplemented with the appropriate antibiotics. For isolating *E. coli* from fecal samples for genomic or plasmid DNA analysis, 10 µl to 50 µl of the fecal suspension was streaked on agar, and single colonies were further streak-purified.

Construction of CRISPR-Cas9 phagemid vectors. Cultures were grown in LB or TB media supplemented with the appropriate antibiotics. Plasmid DNA was prepared by QIAprep Spin

Miniprep Kit (Qiagen 27106), eluted in TE buffer, and incubated at 60 °C for 10 minutes. Samples were quantified using a NanoDrop One spectrophotometer. The vector pCas9 [59] was digested with BsaI (NEB R0535) and gel extracted with a QIAquick Gel Extraction Kit (Qiagen 28706). Spacers were generated by annealing and phosphorylating the two oligos (PSP116 and PSP117 for GFPT; PSP120 and PSP121 for NT [66]) at 10 µM each in T4 ligation buffer (NEB B0202S) with T4 polynucleotide kinase (NEB M0201S) by incubating at 37 °C for 2 hours, 95 °C for 5 minutes, and ramping down to 20 °C at 5 °C/min. The annealed product was diluted 1 in 200 in sterile distilled water and used for directional cloning by ligating (Thermo Scientific FEREL0011) to 60 ng of BsaI-digested, gel extracted pCas9 overnight at room temperature. Ligations were used to transform 5-alpha competent cells (NEB C2987H) and the cloned spacer was verified by Sanger sequencing using primer PSP108. The trailing repeat was later confirmed to lack the starting 5'G, which did not interfere with GFP-targeting function. The 1.8-kb fragment carrying the f1 origin of replication and beta-lactamase gene (f1-*bla*) was amplified from pBluescript II with SalI adapters using primers KL215 and KL216 and KOD Hot Start DNA polymerase (Millipore 71842-3). The PCR product was purified using a QIAquick PCR Purification Kit (Qiagen 28104), digested with SalI (Thermo Fisher FD0644), gel extracted, and used to ligate to SalI-digested, FastAP-dephosphorylated (Thermo Fisher FEREF0651) vector. Ligations were used to transform DH5alpha and clones were screened by restriction digest for both possible insert orientations (A or B) using XbaI (Thermo Scientific FD0684) and one of each orientation was saved for both the GFPT and NT phagemids.

Preparation of M13 carrying pBluescript II. This protocol was adapted from those to generate phage display libraries [79]. XL1-Blue MRF' was transformed with pBluescript II (Agilent 212208). An overnight culture of this strain was prepared in 5 ml LB supplemented with tetracycline (5 µg/ml) and carbenicillin (50 µg/ml) and subcultured the following day 1-in-100 into 5 ml 2YT supplemented with the same antibiotics. At an OD_{600} of 0.8, cells were infected with helper phage M13KO7 (NEB N0315S) at a multiplicity of infection of approximately 10:1 for 1 h at 37 °C. The infected cells were used to seed 2YT supplemented with carbenicillin (100 µg/ml) and kanamycin (25 µg/ml) at 1-in-100, and the culture was grown overnight to produce phage. Cells were pelleted at 10,000×g for 15 minutes, and the supernatant containing phage was transferred. Phage were precipitated by adding 0.2 volumes phage precipitation solution (20% PEG-8000, 2.5 M NaCl), inverting to mix well, and incubating for 30 minutes on ice. Phage were pelleted at 15,000×g for 15 minutes at 4 °C and the supernatant was discarded. The phage pellet was resuspended in PBS at 1-4% of the culture volume. The resuspension was centrifuged to pellet insoluble material and transferred to a new tube. Glycerol was added to a final concentration of 10-15%. Phage preparations were aliquoted into cryovials and frozen at –80 °C for long-term storage.

Preparation of M13 carrying CRISPR-Cas9 phagemids. DH5alpha(HP4_M13) [69] was transformed with the GFPT phagemid (pCas9-GFPT-f1A or pCas9-GFPT-f1B) or the NT phagemid (pCas9-GFPT-f1A or pCas9-GFPT-f1B) and plated on LB media containing carbenicillin and kanamycin. Transformants were inoculated into 5 ml 2YT supplemented with 100 µg/ml carbenicillin and 25 µg/ml kanamycin, incubated overnight, used 1-in-100 to seed 250 ml of the same media, and incubated overnight. Cells were pelleted at 10,000×g for 15 minutes, the supernatant was transferred to a new tube, 0.2 volumes of phage precipitation solution was added, and incubated 30 minutes on ice. Phage were pelleted at 20,000×g for 20 minutes with slow deceleration. The supernatant was completely removed, phage were resuspended in PBS at 1% of the culture volume, and glycerol was added to a final concentration of 10-15%. The phage solution was centrifuged at 21,000×g to pellet insoluble matter, filtered through 0.45 µm, and stored at –80 °C.

Titration of M13 phage carrying phagemid DNA. Phage titer was determined using indicator strain XL1-Blue MRF’ or Sm^R W1655 F+. An overnight culture of the indicator strain in LB supplemented with the appropriate antibiotics was subcultured 1-in-100 or 1-in-200 into fresh media and grown to an OD_{600} of 0.8. To estimate titer, serial ten-fold dilutions of the phage preparation were made in PBS, and 10 µl of each dilution was used to infect 90 µl of cells. After incubating at 37 °C for 30 minutes with shaking, 10 µl of the infection mix was spotted onto LB supplemented with carbenicillin. For more accurate titration, 100 µl of phage dilutions were mixed with 900 µl cells in culture tubes, incubated at 37 °C for 30 minutes with shaking, and 100 µl was plated on LB carbenicillin.

Targeting experiments *in vitro* with M13 CRISPR-Cas9. Overnight cultures of fluorescently marked Sm^R W1655 F+ *sfgfp* and *mcherry* were prepared in LB supplemented with streptomycin, subcultured 1 in 200 into fresh media, and grown to an OD_{600} of 0.8. 900 µl cells (approximately 1×10^9) was transferred to a culture tube, 100 µl phage (approximately 1×10^{10} for f1A vectors and approximately 5×10^{10} for f1B vectors) was added, and the tube was incubated at 37 °C for 30 minutes. The infection culture was transferred to a microfuge tube, cells were pelleted at 21,000×g for 1 minute, and the supernatant was removed. Cells were washed twice by adding 1 ml PBS, vortexing, pelleting cells, and removing supernatant. Cells were resuspended in 1 ml PBS, and ten-fold serially diluted in PBS. 10 µl of each dilution was spotted onto LB supplemented with carbenicillin and 100 µl was plated on larger plates for isolating single colonies for analysis. Colonies were picked and streak-purified four times to ensure phenotypic homogeneity and clonality.

Co-culture experiments with *sfgfp* and *mcherry* infected with M13 CRISPR-Cas9. Overnight cultures of fluorescently marked Sm^R W1655 F+ *sfgfp* and *mcherry* were prepared in LB supplemented with streptomycin. For each culture, three serial ten-fold dilutions were made in PBS, followed by a fourth ten-fold dilution into LB. Equal volumes of each were combined and 5 ml aliquots were transferred to culture tubes. Using a CFU assay, the input was determined to be

6×10^6 CFU of each strain or 1×10^7 CFU total. 10 µl (5×10^9) M13 carrying CRISPR-Cas9 was added, the co-culture was incubated at 37 °C for 30 minutes, and carbenicillin was added to a final concentration of 100 µg/ml. The co-culture was sampled for the t = 0 timepoint and then incubated for 24 hours with further sampling every 4 hours. At each timepoint, 200 µl was taken; 100 µl was used to assay carbenicillin in the media (see below) and the remaining 100 µl was used for plating as follows. To the 100 µl sample of culture, 900 µl was added and cells were washed by vortexing. Cells were pelleted by centrifuging at 21,000×g for 1 min, and 900 µl of the supernatant was removed. To remove residual phage and antibiotic, the wash was repeated once more by adding 900 µl PBS, vortexing, pelleting cells, and removing 900 µl. Cells were resuspended in the remaining 100 µl. Serial ten-fold dilutions were made in PBS and 10 µl of each dilution was spotted onto LB or LB carbenicillin.

Carbenicillin bioassay. Cultures were sampled over time, cells were pelleted at 21,000×g for 1 minute, and the supernatant was transferred to a new tube and frozen at –20 °C until all timepoints were collected. The supernatants were thawed and assayed using a Kirby-Bauer disk diffusion test. An overnight culture of the indicator organism (*Bacillus subtilis 168*) was diluted in saline to an OD_{600} of 0.1. A cotton swab was dipped into this dilution and spread across LB agar, antibiotic sensitivity disks (Fisher Scientific S70150A) were overlaid using tweezers, and 20 µl of the supernatant was applied to the disk. At the same time, carbenicillin standards were prepared from 1 µg/ml to 100 µg/ml and also applied to discs. Plates were incubated overnight at 37 °C and imaged the following morning.

Treatment of mice with phage. Filtered phage solutions stored at –80 °C were thawed and used directly. Unfiltered phage solutions were precipitated by diluting approximately 5-fold in PBS, adding 0.2 volumes phage precipitation solution, incubating for 15 minutes on ice, pelleting at 15,000–21,000×g for 15 minutes at 4 °C, resuspending in PBS, centrifuging to pellet insoluble matter, and filtering through 0.45 µm. Heat-inactivated phage were prepared by incubating 1 ml aliquots at 95 °C in a water bath for 30 minutes. Streptomycin-treated mice colonized with Sm^R *E. coli* were orally gavaged with 0.2 ml of phage and placed on drinking water containing both streptomycin and carbenicillin.

Flow cytometry. For turbid *in vitro* cultures, samples were diluted 1 in 10,000 in PBS. For mouse fecal pellets, samples were used fresh or thawed from –80 °C, and suspended in 500 µl PBS by manual mixing and vortexing. Fecal suspensions were incubated aerobically at 4 °C overnight to improve fluorescence signal (Figure S17). Samples were vortexed to mix, large particulate matter was pelleted by centrifuging at 100×g for 30 seconds, and the sample was diluted 1-in-100 in PBS. Samples were run on a BD LSRFortessa DUAL flow cytometer using a 530/30 nm filter for GFP fluorescence and 610/20 nm for mCherry fluorescence, with the following voltages: 750 V for FSC, 400 V for SSC, 700 V for mCherry, and 700-800 V (*in vivo*) or 650 V (*in vitro*) for GFP. Flow cytometry data were analyzed in R using packages *flowCore* v1.52.1 [80], *Phenoflow* v1.1.2 [81], and *ggcyto* v1.14.0 [82]. Typically, between 10,000 and 100,000 events were collected per sample, and data were rarefied after gating on FSC and SSC.

Analysis of plasmid DNA and genomic DNA from *in vitro* or *in vivo* isolates. Fecal suspensions in PBS or saline were cultured on LB or Difco MacConkey agar plates supplemented with the appropriate antibiotics. Colonies were picked, streak-purified, and inoculated into LB or TB supplemented with the appropriate antibiotics. Plasmid DNA was extracted using a QIAprep Spin Miniprep Kit (Qiagen 27106), eluted in TE buffer, and incubated at 60 °C for 10 minutes. Samples were quantified using a NanoDrop One spectrophotometer and 200-600 ng was digested with FastDigest restriction enzymes (KpnI, Thermo Scientific FD0524; XbaI, Thermo Scientific FD0684) for 10 minutes at 37 °C followed by gel electrophoresis. Spacer sequences on phagemids were confirmed by Sanger sequencing using primer PSP108. Genomic DNA was extracted crudely to use as template for PCR. Briefly, 1.5 ml to 3 ml of culture was transferred to a microfuge tube, cells were pelleted by centrifuging, and the supernatant was discarded. The pellet was frozen, allowed to thaw on ice, resuspended in 100 µl TE, and incubated at 100 °C for 15 minutes in an Eppendorf ThermoMixer. Samples were cooled on ice, cell debris was pelleted by centrifuging at 21,000×g for 1 minute, the supernatant was transferred to a new tube, and diluted 1-in-100 in TE to use as template DNA. PCR was performed using KOD Hot Start DNA polymerase (Millipore 71842-3) using primers KL207 and KL200 for PCR of the *sfgfp* gene and primers BAC338F and BAC805R for the 16S rRNA gene [83].

References

1. Shepherd, E. S., DeLoache, W. C., Pruss, K. M., Whitaker, W. R. & Sonnenburg, J. L. An exclusive metabolic niche enables strain engraftment in the gut microbiota. *Nature* **557**, 434–438 (2018).
2. Kearney, S. M., Gibbons, S. M., Erdman, S. E. & Alm, E. J. Orthogonal dietary niche enables reversible engraftment of a gut bacterial commensal. *Cell Rep.* **24**, 1842–1851 (2018).
3. Staley, C. *et al.* Stable engraftment of human microbiota into mice with a single oral gavage following antibiotic conditioning. *Microbiome* **5**, 87 (2017).
4. Thompson, J. A., Oliveira, R. A., Djukovic, A., Ubeda, C. & Xavier, K. B. Manipulation of the quorum sensing signal AI-2 affects the antibiotic-treated gut microbiota. *Cell Rep.* **10**, 1861–1871 (2015).
5. Isabella, V. M. *et al.* Development of a synthetic live bacterial therapeutic for the human metabolic disease phenylketonuria. *Nat. Biotechnol.* **36**, 857–864 (2018).
6. Kurtz, C. B. *et al.* An engineered e. coli nissle improves hyperammonemia and survival in mice and shows dose-dependent exposure in healthy humans. *Sci. Transl. Med.* **11** (2019).
7. Zhu, W. *et al.* Precision editing of the gut microbiota ameliorates colitis. *Nature* **553**, 208–211 (2018).
8. Wallace, B. D. *et al.* Alleviating cancer drug toxicity by inhibiting a bacterial enzyme. *Science* **330**, 831–835 (2010).
9. Mimee, M., Tucker, A. C., Voigt, C. A. & Lu, T. K. Programming a human commensal bacterium, *Bacteroides thetaiotaomicron*, to sense and respond to stimuli in the murine gut microbiota. *Cell Systems* **1**, 62–71 (2015).
10. Lim, B., Zimmermann, M., Barry, N. A. & Goodman, A. L. Engineered regulatory systems modulate gene expression of human commensals in the gut. *Cell* **169**, 547–558.e15 (2017).
11. Ronda, C., Chen, S. P., Cabral, V., Yaung, S. J. & Wang, H. H. Metagenomic engineering of the mammalian gut microbiome in situ. *Nat. Methods* **16**, 167–170 (2019).
12. Rodrigues, M., McBride, S. W., Hullahalli, K., Palmer, K. L. & Duerkop, B. A. Conjugative delivery of CRISPR-Cas9 for the selective depletion of antibiotic-resistant enterococci. *Antimicrob. Agents Chemother.* AAC.01454–19 (2019).
13. Merril, C. R., Scholl, D. & Adhya, S. L. The prospect for bacteriophage therapy in western medicine. *Nat. Rev. Drug Discov.* **2**, 489–497 (2003).
14. Abedon, S. T., Kuhl, S. J., Blasdel, B. G. & Kutter, E. M. Phage treatment of human infections. *Bacteriophage* **1**, 66–85 (2011).
15. Lu, T. K. & Koeris, M. S. The next generation of bacteriophage therapy. *Curr. Opin. Microbiol.* **14**, 524–531 (2011).

16. Brüssow, H. Phage therapy for the treatment of human intestinal bacterial infections: soon to be a reality? *Expert Rev. Gastroenterol. Hepatol.* **11**, 785–788 (2017).
17. Abedon, S. T., García, P., Mullany, P. & Aminov, R. Editorial: Phage therapy: Past, present and future. *Front. Microbiol.* **8**, 981 (2017).
18. Maura, D. *et al.* Intestinal colonization by enteroaggregative escherichia coli supports long-term bacteriophage replication in mice. *Environ. Microbiol.* **14**, 1844–1854 (2012).
19. Weiss, M. *et al.* In vivo replication of T4 and T7 bacteriophages in germ-free mice colonized with escherichia coli. *Virology* **393**, 16–23 (2009).
20. Chibani-Chennoufi, S. *et al.* In vitro and in vivo bacteriolytic activities of escherichia coli phages: implications for phage therapy. *Antimicrob. Agents Chemother.* **48**, 2558–2569 (2004).
21. Maura, D., Galtier, M., Le Bouguénec, C. & Debarbieux, L. Virulent bacteriophages can target O104:H4 enteroaggregative escherichia coli in the mouse intestine. *Antimicrob. Agents Chemother.* **56**, 6235–6242 (2012).
22. Porter, N. T. *et al.* Phase-variable capsular polysaccharides and lipoproteins modify bacteriophage susceptibility in bacteroides thetaiotaomicron (2020).
23. Citorik, R. J., Mimee, M. & Lu, T. K. Sequence-specific antimicrobials using efficiently delivered RNA-guided nucleases. *Nat. Biotechnol.* **32**, 1141–1145 (2014).
24. Bikard, D. *et al.* Exploiting CRISPR-Cas nucleases to produce sequence-specific antimicrobials. *Nat. Biotechnol.* **32**, 1146–1150 (2014).
25. Park, J. Y. *et al.* Genetic engineering of a temperate phage-based delivery system for CRISPR/Cas9 antimicrobials against staphylococcus aureus. *Sci. Rep.* **7**, 44929 (2017).
26. Selle, K. *et al.* In vivo targeting of clostridioides difficile using Phage-Delivered CRISPR-Cas3 antimicrobials. *MBio* **11** (2020).
27. Shkoporov, A. N. & Hill, C. Bacteriophages of the human gut: The “known unknown” of the microbiome. *Cell Host Microbe* **25**, 195–209 (2019).
28. Reyes, A., Semenkovich, N. P., Whiteson, K., Rohwer, F. & Gordon, J. I. Going viral: next-generation sequencing applied to phage populations in the human gut. *Nat. Rev. Microbiol.* **10**, 607–617 (2012).
29. Brüssow, H. Environmental microbiology: Too much food for thought? - an argument for reductionism. *Environ. Microbiol.* (2018).
30. Hofschneider, P. H. Untersuchungen über kleine“ e. coli K 12 bakteriophagen. *Zeitschrift für Naturforschung B* **18**, 203–210 (1963).
31. Ackermann, H.-W. Phage classification and characterization. *Methods Mol. Biol.* **501**, 127–140 (2009).
32. Salivar, W. O., Tzagoloff, H. & Pratt, D. Some Physical-Chemical and biological properties of the Rod-Shaped coliphage M13. *Virology* **24**, 359–371 (1964).

33. Lee, G. S. & Ames, G. F. Analysis of promoter mutations in the histidine transport operon of salmonella typhimurium: use of hybrid M13 bacteriophages for cloning, transformation, and sequencing. *J. Bacteriol.* **159**, 1000–1005 (1984).

34. Lin, A. *et al.* Inhibition of bacterial conjugation by phage M13 and its protein g3p: quantitative analysis and model. *PLoS One* **6**, e19991 (2011).

35. Yanisch-Perron, C., Vieira, J. & Messing, J. Improved M13 phage cloning vectors and host strains: nucleotide sequences of the m13mp18 and pUC19 vectors. *Gene* **33**, 103–119 (1985).

36. Sanger, F., Coulson, A. R., Barrell, B. G., Smith, A. J. & Roe, B. A. Cloning in single-stranded bacteriophage as an aid to rapid DNA sequencing. *J. Mol. Biol.* **143**, 161–178 (1980).

37. Zoller, M. J. & Smith, M. Oligonucleotide-directed mutagenesis using m13-derived vectors: an efficient and general procedure for the production of point mutations in any fragment of DNA. *Nucleic Acids Res.* **10**, 6487–6500 (1982).

38. Smith, G. P. & Petrenko, V. A. Phage display. *Chem. Rev.* **97**, 391–410 (1997).

39. Sidhu, S. S. Engineering M13 for phage display. *Biomol. Eng.* **18**, 57–63 (2001).

40. Roux, S. *et al.* Cryptic inoviruses revealed as pervasive in bacteria and archaea across earth's biomes. *Nature Microbiology* **4**, 1895–1906 (2019).

41. Pasqualini, R. & Ruoslahti, E. Organ targeting in vivo using phage display peptide libraries. *Nature* **380**, 364–366 (1996).

42. Rajotte, D. *et al.* Molecular heterogeneity of the vascular endothelium revealed by in vivo phage display. *J. Clin. Invest.* **102**, 430–437 (1998).

43. Krag, D. N. *et al.* Phage-displayed random peptide libraries in mice: toxicity after serial panning. *Cancer Chemother. Pharmacol.* **50**, 325–332 (2002).

44. Westwater, C. *et al.* Use of genetically engineered phage to deliver antimicrobial agents to bacteria: an alternative therapy for treatment of bacterial infections. *Antimicrob. Agents Chemother.* **47**, 1301–1307 (2003).

45. Lu, T. K. & Collins, J. J. Engineered bacteriophage targeting gene networks as adjuvants for antibiotic therapy. *Proc. Natl. Acad. Sci. U. S. A.* **106**, 4629–4634 (2009).

46. Cao, J. *et al.* Helicobacter pylori-antigen-binding fragments expressed on the filamentous M13 phage prevent bacterial growth. *Biochim. Biophys. Acta* **1474**, 107–113 (2000).

47. Miller, C. P. & Bohnhoff, M. Changes in the mouse's enteric microflora associated with enhanced susceptibility to salmonella infection following streptomycin treatment. *J. Infect. Dis.* **113**, 59–66 (1963).

48. Myhal, M. L., Laux, D. C. & Cohen, P. S. Relative colonizing abilities of human fecal and K 12 strains of escherichia coli in the large intestines of streptomycin-treated mice. *Eur. J. Clin. Microbiol.* **1**, 186–192 (1982).

49. Leatham, M. P. *et al.* Precolonized human commensal escherichia coli strains serve as a barrier to e. coli O157:H7 growth in the streptomycin-treated mouse intestine. *Infect. Immun.* **77**, 2876–2886 (2009).

50. Alting-Mees, M. A. & Short, J. M. pbluescript II: gene mapping vectors. *Nucleic Acids Res.* **17**, 9494 (1989).

51. Kimura, T. & Higaki, K. Gastrointestinal transit and drug absorption. *Biol. Pharm. Bull.* **25**, 149–164 (2002).

52. Coste, M., Gouet, P. & Escoula, L. Ampicillin inactivation in the caecum of axenic, gnotoxenic and conventional lambs: interaction with resistant or sensitive escherichia coli. *J. Gen. Microbiol.* **130**, 1325–1330 (1984).

53. van der Waaij, D., de Vries-Hospers, H. G. & Welling, G. W. The influence of antibiotics on gut colonization. *J. Antimicrob. Chemother.* **18 Suppl C**, 155–158 (1986).

54. Corpet, D. E., Lumeau, S. & Corpet, F. Minimum antibiotic levels for selecting a resistance plasmid in a gnotobiotic animal model. *Antimicrob. Agents Chemother.* **33**, 535–540 (1989).

55. Reikvam, D. H. *et al.* Depletion of murine intestinal microbiota: effects on gut mucosa and epithelial gene expression. *PLoS One* **6**, e17996 (2011).

56. Duval-Iflah, Y., Raibaud, P., Tancrede, C. & Rousseau, M. R-plasmic transfer from serratia liquefaciens to escherichia coli in vitro and in vivo in the digestive tract of gnotobiotic mice associated with human fecal flora. *Infect. Immun.* **28**, 981–990 (1980).

57. Jończyk, E., Kłak, M., Miedzybrodzki, R. & Górski, A. The influence of external factors on bacteriophages–review. *Folia Microbiol.* **56**, 191–200 (2011).

58. Tóthová, L., Bábíčková, J. & Celec, P. Phage survival: the biodegradability of M13 phage display library in vitro. *Biotechnol. Appl. Biochem.* **59**, 490–494 (2012).

59. Jiang, W., Bikard, D., Cox, D., Zhang, F. & Marraffini, L. A. RNA-guided editing of bacterial genomes using CRISPR-Cas systems. *Nat. Biotechnol.* **31**, 233–239 (2013).

60. Cui, L. & Bikard, D. Consequences of cas9 cleavage in the chromosome of escherichia coli. *Nucleic Acids Res.* **44**, 4243–4251 (2016).

61. Gynnå, A. H., Wiktor, J., Leroy, P. & Elf, J. RecA mediated homology search finds segregated sister locus in minutes after a double stranded break (2020).

62. Yosef, I., Manor, M., Kiro, R. & Qimron, U. Temperate and lytic bacteriophages programmed to sensitize and kill antibiotic-resistant bacteria. *Proceedings of the National Academy of Sciences* **112**, 201500107 (2015).

63. Bikard, D. & Barrangou, R. Using CRISPR-Cas systems as antimicrobials. *Curr. Opin. Microbiol.* **37**, 155–160 (2017).

64. Bethesda Research Laboratories. BRL pUC host: *E. coli* DH5α competent cells. *Focus* **8**, 8 (1986).

65. Bachmann, B. J. Derivations and genotypes of some mutant derivatives of escherichia coli K-12. In Neidhardt, F. C. e. a. (ed.) *Escherichia coli and Salmonella typhimurium: Cellular and Molecular Biology* (ASM Press, Washington, DC, 1996).

66. Vigouroux, A., Oldewurtel, E., Cui, L., Bikard, D. & van Teeffelen, S. Tuning dcas9's ability to block transcription enables robust, noiseless knockdown of bacterial genes. *Mol. Syst. Biol.* **14**, e7899 (2018).

67. Jensen, S. I., Lennen, R. M., Herrgård, M. J. & Nielsen, A. T. Seven gene deletions in seven days: Fast generation of escherichia coli strains tolerant to acetate and osmotic stress. *Sci. Rep.* **5**, 17874 (2015).

68. St-Pierre, F. *et al.* One-step cloning and chromosomal integration of DNA. *ACS Synth. Biol.* **2**, 537–541 (2013).

69. Praetorius, F. *et al.* Biotechnological mass production of DNA origami. *Nature* **552**, 84–87 (2017).

70. Gohl, D. M. *et al.* Systematic improvement of amplicon marker gene methods for increased accuracy in microbiome studies. *Nat. Biotechnol.* **34**, 942–949 (2016).

71. Bisanz, J. 16S rRNA amplicon sequencing pipeline. `https://github.com/jbisanz/16Spipelines/blob/master/QIIME2_pipeline.Rmd`.

72. Bolyen, E. *et al.* Reproducible, interactive, scalable and extensible microbiome data science using QIIME 2. *Nat. Biotechnol.* **37**, 852–857 (2019).

73. Callahan, B. J. *et al.* DADA2: High-resolution sample inference from illumina amplicon data. *Nat. Methods* **13**, 581–583 (2016).

74. Bisanz, J. qiime2r. `https://github.com/jbisanz/qiime2R`.

75. McMurdie, P. J. & Holmes, S. phyloseq: an R package for reproducible interactive analysis and graphics of microbiome census data. *PLoS One* **8**, e61217 (2013).

76. Smith, S. D. phylosmith: an r-package for reproducible and efficient microbiome analysis with phyloseq-objects. *Journal of Open Source Software* **4**, 1442 (2019).

77. Datsenko, K. a. & Wanner, B. L. One-step inactivation of chromosomal genes in escherichia coli K-12 using PCR products. *Proc. Natl. Acad. Sci. U. S. A.* **97**, 6640–6645 (2000).

78. Timms, A. R., Steingrimsdottir, H., Lehmann, A. R. & Bridges, B. A. Mutant sequences in the rpsl gene of escherichia coli b/r: mechanistic implications for spontaneous and ultraviolet light mutagenesis. *Mol. Gen. Genet.* **232**, 89–96 (1992).

79. Tonikian, R., Zhang, Y., Boone, C. & Sidhu, S. S. Identifying specificity profiles for peptide recognition modules from phage-displayed peptide libraries. *Nat. Protoc.* **2**, 1368–1386 (2007).

80. Hahne, F. *et al.* flowcore: a bioconductor package for high throughput flow cytometry. *BMC Bioinformatics* **10**, 106 (2009).

81. Props, R., Monsieurs, P., Mysara, M., Clement, L. & Boon, N. Measuring the biodiversity of microbial communities by flow cytometry. *Methods Ecol. Evol.* **7**, 1376–1385 (2016).

82. Van, P., Jiang, W., Gottardo, R. & Finak, G. ggcyto: next generation open-source visualization software for cytometry. *Bioinformatics* **34**, 3951–3953 (2018).

83. Yu, Y., Lee, C., Kim, J. & Hwang, S. Group-specific primer and probe sets to detect methanogenic communities using quantitative real-time polymerase chain reaction. *Biotechnol. Bioeng.* **89**, 670–679 (2005).

Supplementary Figures

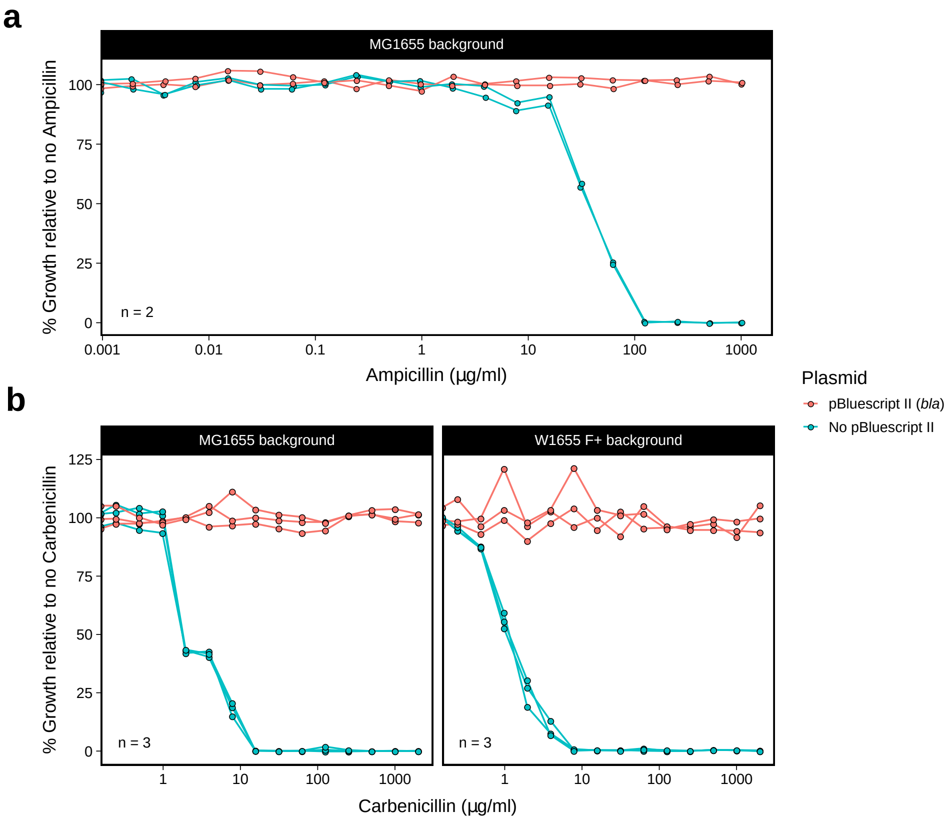

Figure S1. Minimum inhibitory concentration (MIC) assays. (a) The plasmid pBluescript II confers resistance to ampicillin exceeding 1 mg/ml in the *E. coli* MG1655 background. In the absence of the plasmid, the MIC is approximately 100 µg/ml. **(b)** pBluescript II confers resistance to carbenicillin exceeding 2 mg/ml in both the *E. coli* MG1655 and W1655 F+ backgrounds. In the absence of the plasmid, the same strains have an MIC of approximately 10 µg/ml. bla, beta-lactamase.

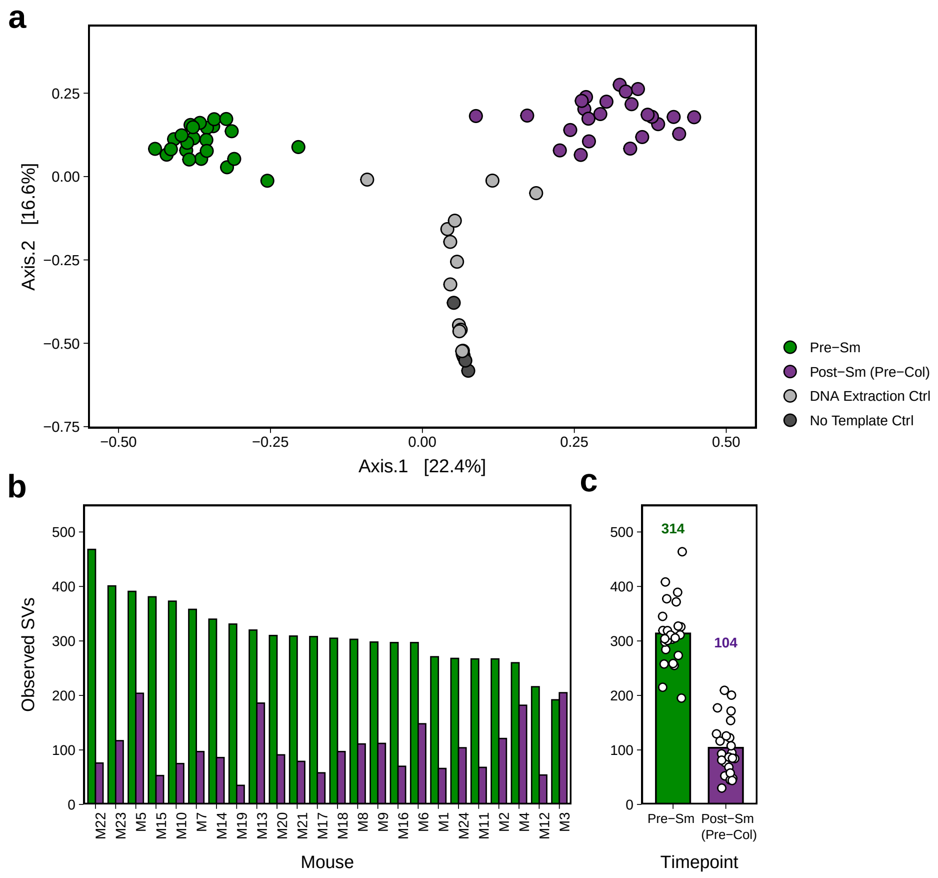

Figure S2. Streptomycin (Sm) treatment reduces bacterial diversity in mice. (a) Principle coordinate analysis (Bray-Curtis) indicates that pre-Sm and post-Sm fecal samples are distinct. **(b)** In a cohort of 24 individually caged mice, Sm treatment generally leads to a decrease in the number of observed 16S rRNA gene sequence variants (SVs) relative to pre-treatment. **(c)** The mean number of observed SVs pre-Sm was 314 while the mean post-Sm (before colonizing with Sm^R *E. coli*) was 104.

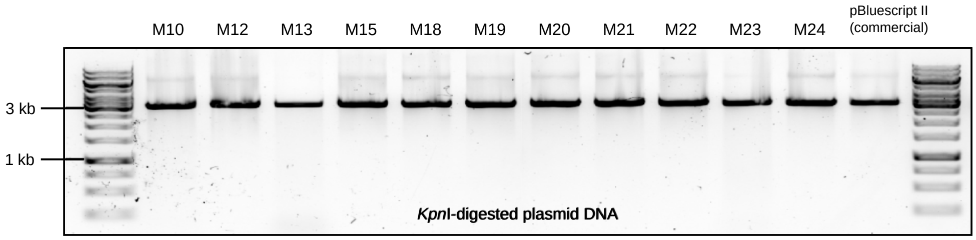

Figure S3. Diagnostic digest of plasmid DNA recovered from *E. coli* in the gut post phage delivery. Plasmid DNA was recovered from Carb^R colonies isolated from the feces of the 11 mice that were successfully colonized during carbenicillin treatment (Figure 1d); DNA was digested with the restriction enzyme KpnI for comparison to linearized 3-kb pBluescript II.

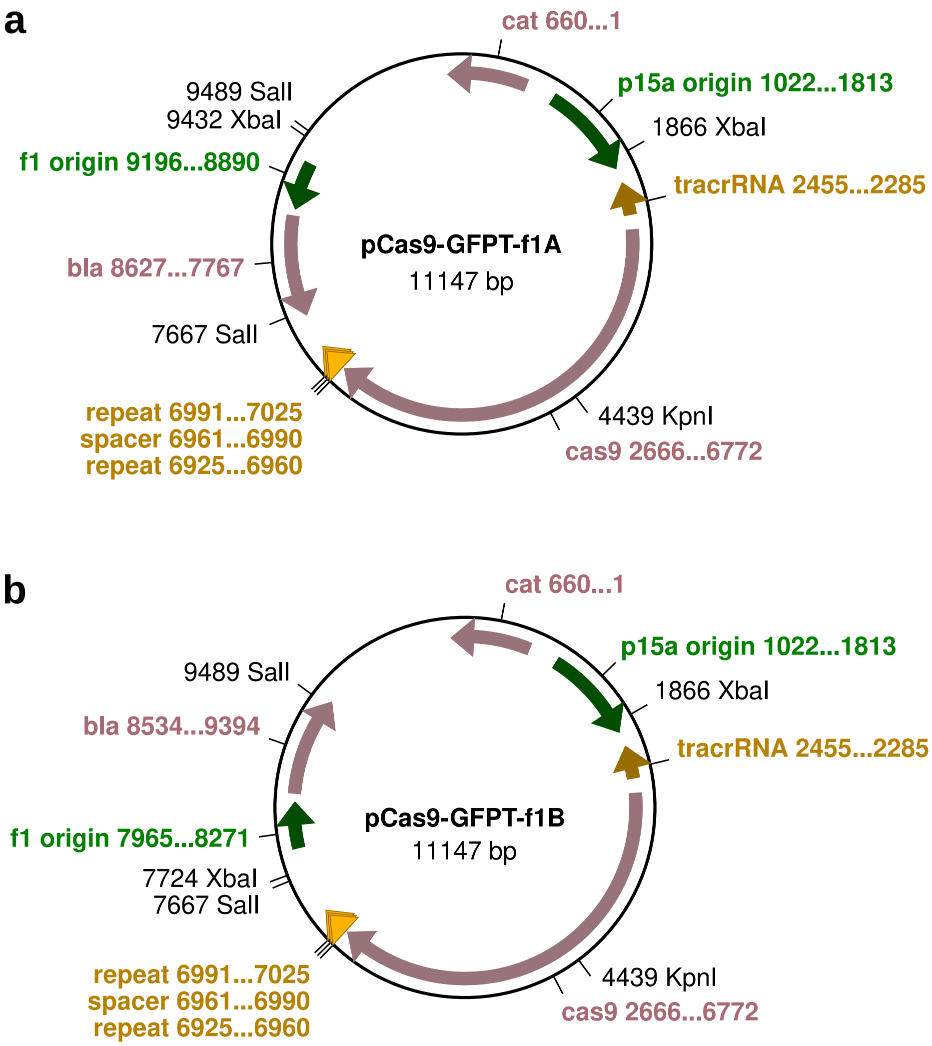

Figure S4. Plasmid maps of GFP-targeting (GFPT) CRISPR-Cas9 vectors. The non-targeting (NT) versions of these vectors (not shown here) are identical to the GFPT vectors except in the spacer sequence. The f1-*bla* fragment was cloned as a SalI fragment in both possible orientations for either strand of DNA to be packaged into M13 phage. **(a)** The first orientation is designated f1A. **(b)** The second orientation is designated f1B. cat, chloramphenicol acetyltranferase (Cm^{R}); bla, beta-lactamase (Carb^{R}).

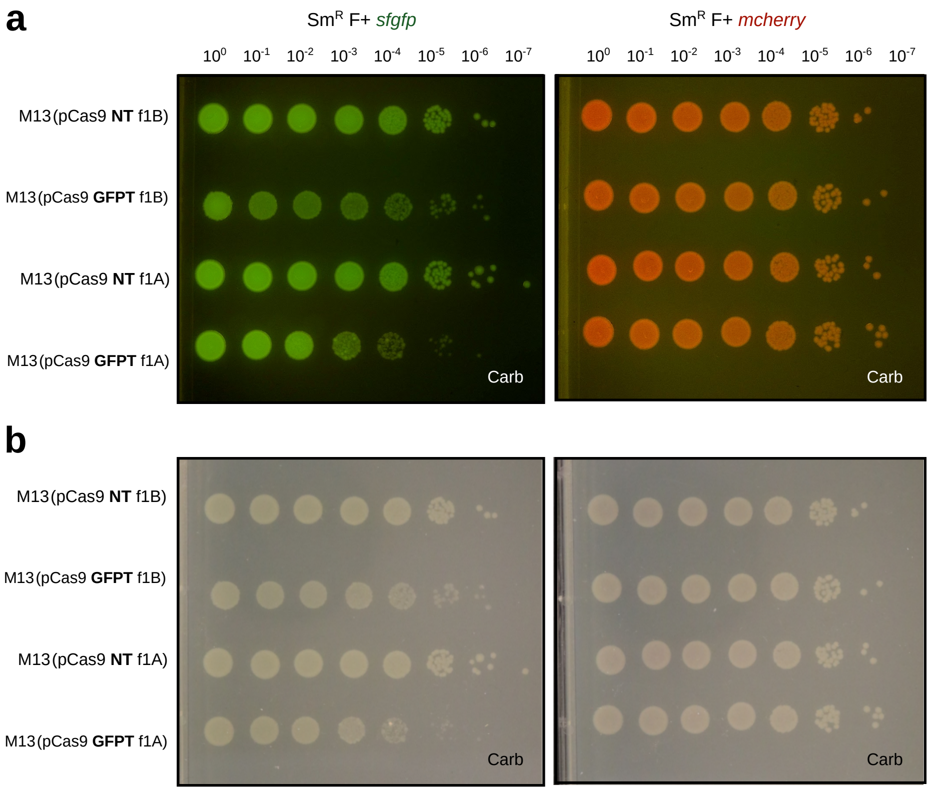

Figure S5. GFP-marked *E. coli* exhibits impaired colony growth after infection with M13 carrying GFP-targeting CRISPR-Cas9. The GFP-marked and mCherry-marked derivatives of Sm^R *E. coli* W6555 F+ were infected with NT M13 or GFPT M13. **(a)** Growth impairment of the GFP-marked strain under GFPT conditions was evident under blue light. **(b)** Impaired colonies exhibited a translucent quality that was more pronounced under white light.

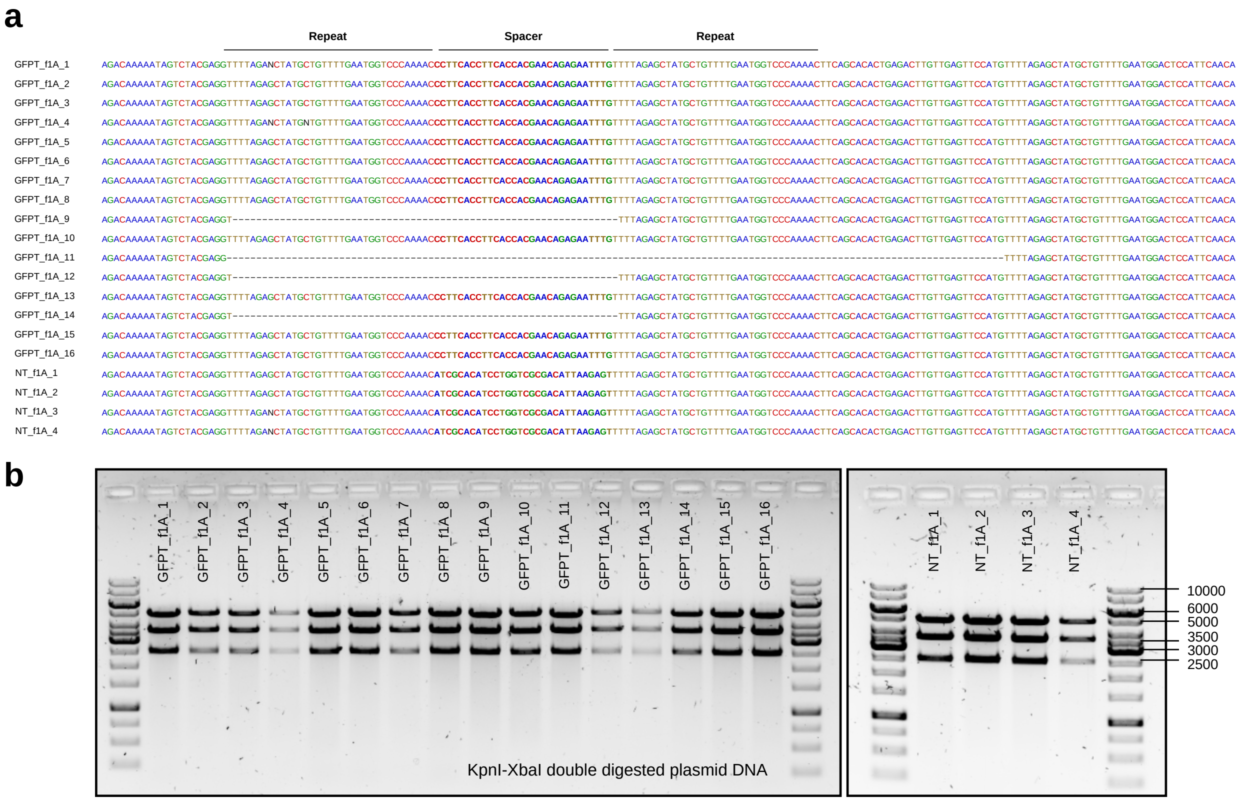

Figure S6. Analysis of CRISPR-Cas9 phagemid DNA from streak-purified clones post M13 targeting *in vitro*. **(a)** Sanger sequencing to confirm spacer presence in phagemid DNA isolates from clones. All 4 clones isolated after infection with NT M13 retained the spacer. Of 16 clones isolated after infection with GFPT M13, 4 had lost the spacer. **(b)** Diagnostic digest of plasmid DNA isolated from clones using KpnI and XbaI revealed phagemid of the expected size. Expected fragments: 4993, 3581, and 2573 bp.

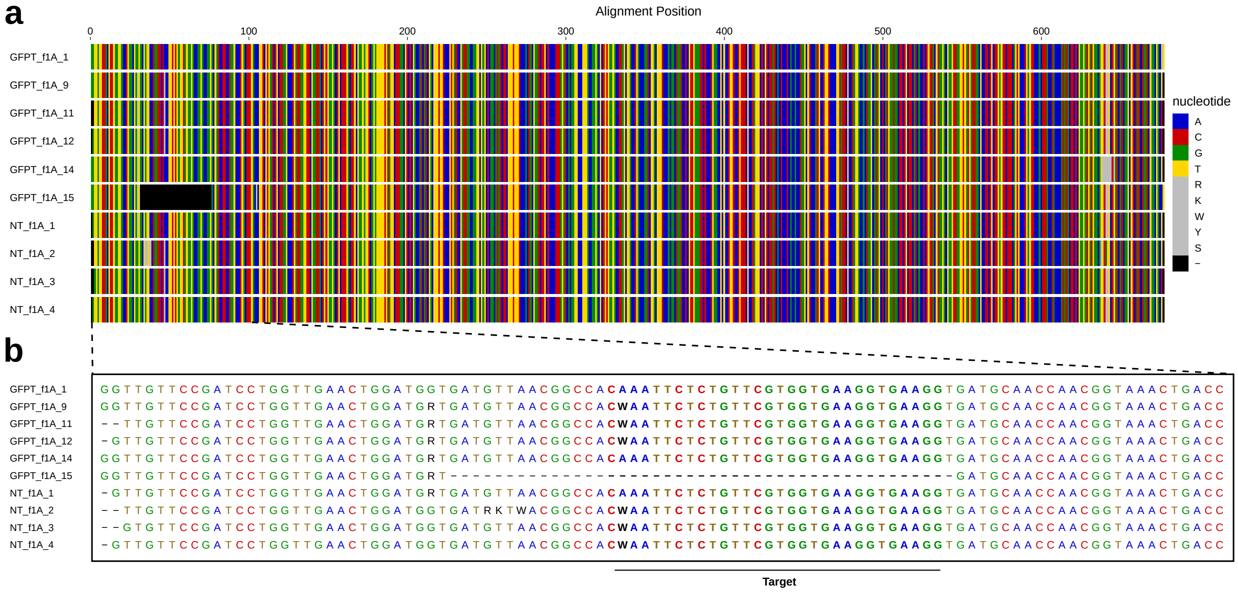

Figure S7. Analysis of *sfgfp* gene from streak-purified clones post M13 targeting *in vitro*. (a) Sanger sequencing of the *sfgfp* PCR amplicons (Figure 2c) confirmed the partial loss observed for clone 15 by gel electrophoresis. **(b)** Pullout: the lost region of the *sfgfp* coding sequence encompasses CRISPR-Cas9 target site.

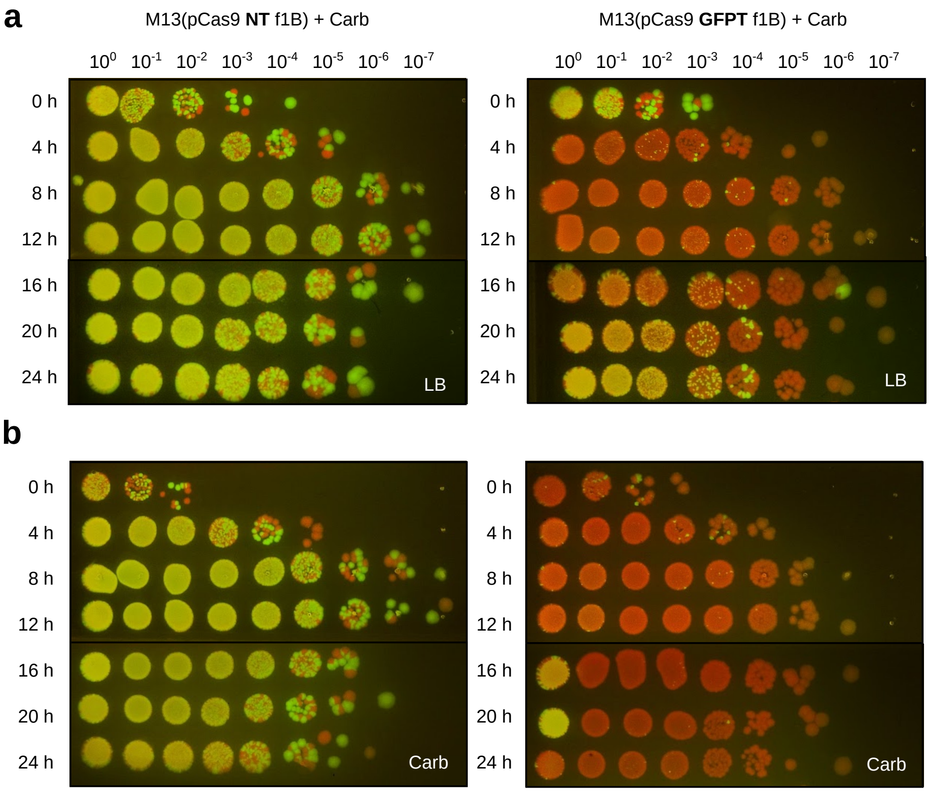

Figure S8. Recovery of GFP+ cells at later timepoints in *in vitro* co-cultures of *sfgfp* and *mcherry E. coli* F+ after infection with GFPT M13 is likey due to lack of selection for CRISPR-Cas9 phagemid. (a) On non-selective media, GFP fluorescent colonies are detected at later timepoints of the co-culture infected with GFPT M13. **(b)** Lack of GFP fluorescent colonies after testing the same co-culture on media with carbenicillin indicates that those GFP+ colonies at later timepoints derives from cells that are Carb^S and suggests that they do not harbour the CRISPR-Cas9 phagemid.

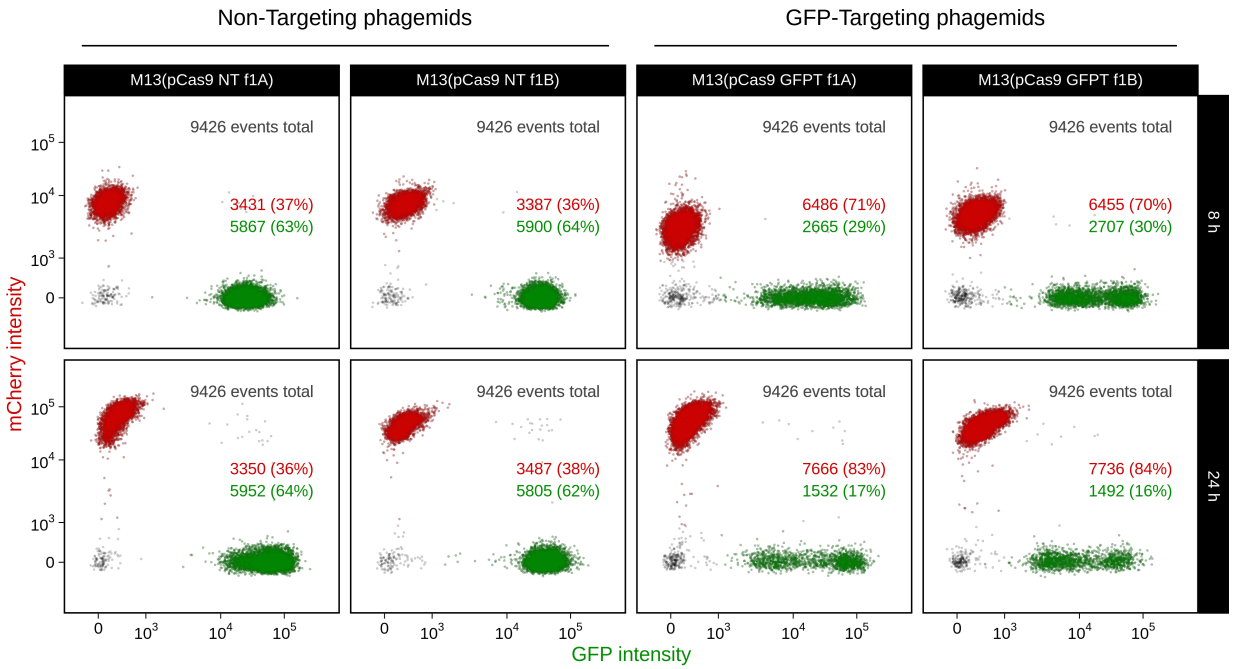

Figure S 9. Flow cytometry on co-cultures at 8 h and 24 h after addition of NT M13 or GFPT M13 shows decreased relative abundance of the GFP strain under targeting conditions. Co-cultures of GFP-marked and mCherry-marked *E. coli* F+ were infected with phage and carbenicillin was added to select for phage infection. The relative abundance of GFP+ events is decreased in GFPT conditions at 8 h and further decreased by 24 h. Non-targeting phagemids are pCas9-NT-f1A and pCas9-NT-f1B; GFP-targeting phagemids are pCas9-GFPT-f1A and pCas9-GFPT-f1B.

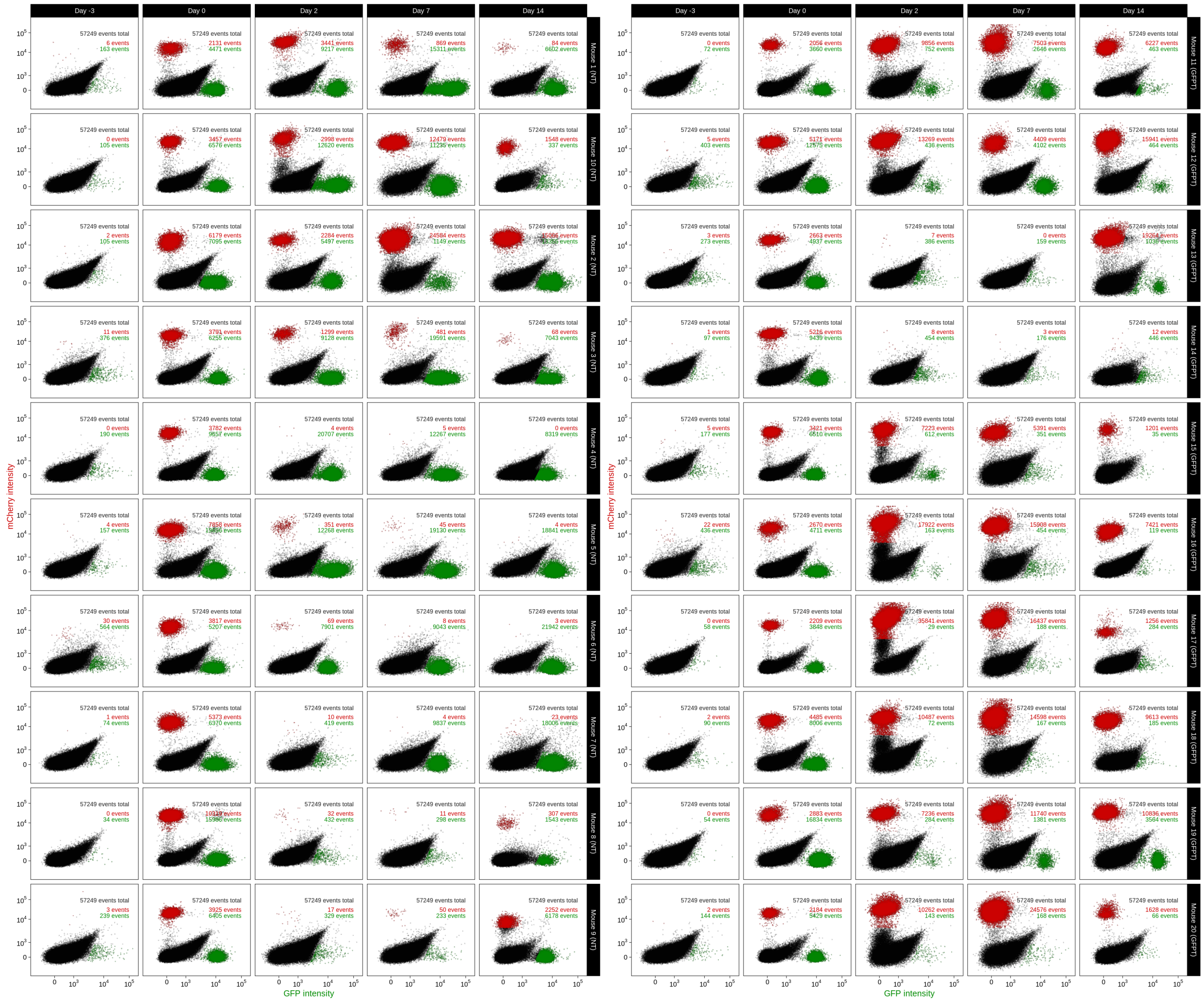

Figure S10. Flow cytometry plots of fecal samples for *in vivo* competition of GFP-marked and mCherry-marked *E. coli* under NT or GFPT conditions for all mice at all timepoints. Mice (n = 10 per group) were given either NT M13 (left) or GFPT M13 (right). Day -3, before engrafting *E. coli*; Day 0, after engraftment with both GFP+ and mCherry+ strains; Day -2, post phage and carbenicillin treatment; Day 7, one week post-phage and carbenicillin; Day -14, one week after removing carbenicillin from drinking water.

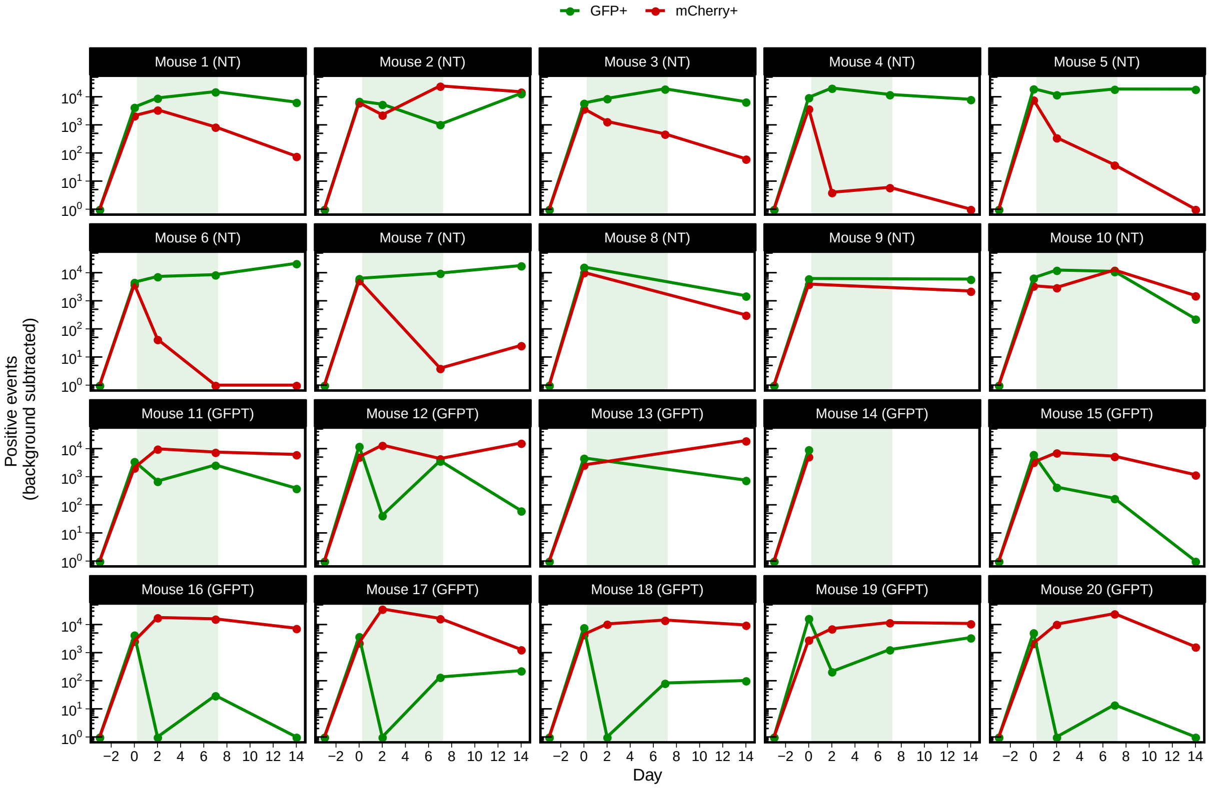

Figure S11. GFP+ and mCherry+ events by flow cytometry in fecal samples over time for individual mice in *in vivo* competition of GFP-marked and mCherry-marked *E. coli* under NT or GFPT conditions. Mice were treated with either NT M13 (M1 to M10) or GFPT M13 (M11 to M20). For each mouse, the number of positive events on Day -3 (before *E. coli* engraftment) was used to subtract background for all subsequent timepoints. Shaded green area indicates duration of carbenicillin treatment. Timepoints were excluded when both mCherry+ and GFP+ events were below background thresholds, calculated as the respective highest observed background on Day -3 multiplied by a factor of 3.

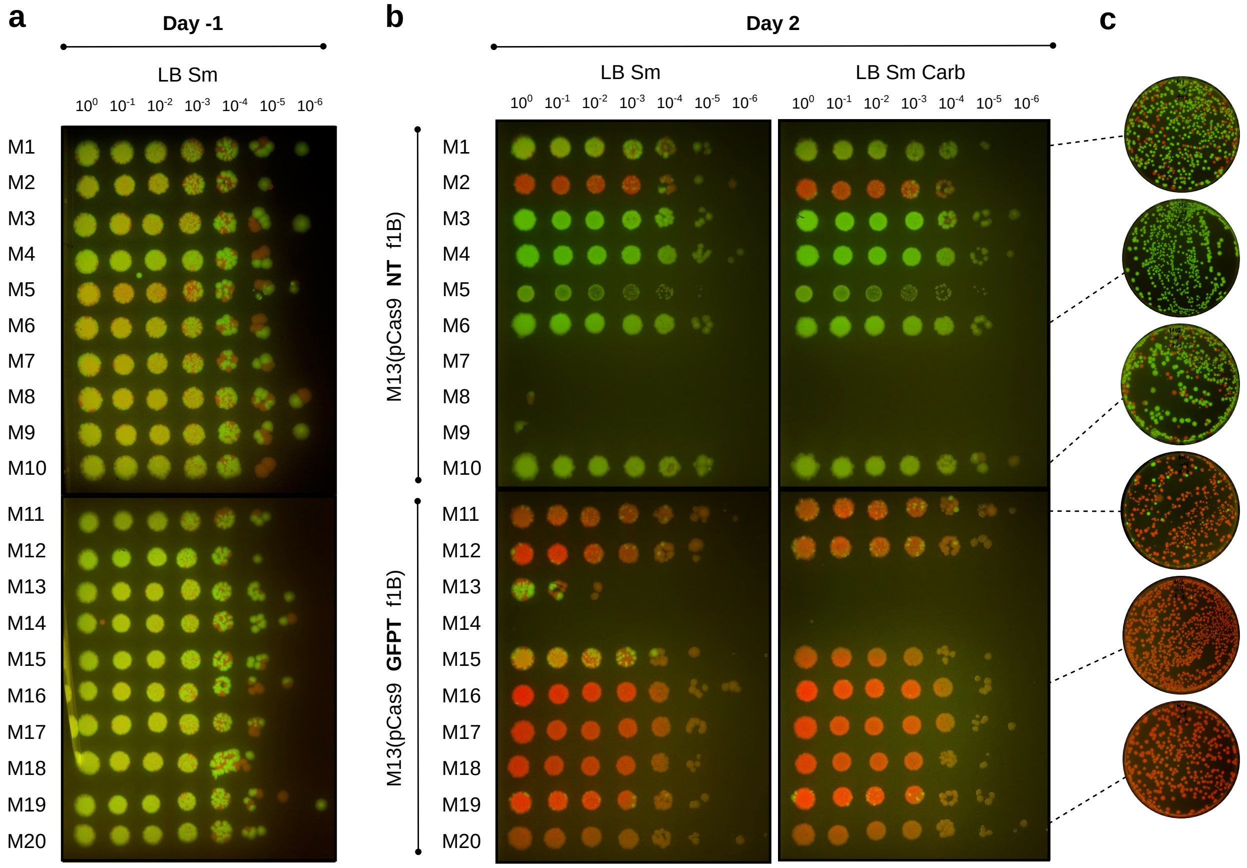

Figure S12. Culturing from fecal samples of mice before (Day -1) or after treatment (Day 2) with NT M13 or GFPT M13 in *in vivo* competition of GFP-marked and mCherry-marked Sm^R *E. coli* F+. (a) At Day -1, engraftment of both the GFP+ and mCherry+ *E. coli* was confirmed in fecal samples of all mice by culturing on LB with streptomycin. **(b)** After treating with NT M13 (M1 to M10) or GFPT M13 (M11 to M20) and carbenicillin to select for phage infection, culture of *E. coli* on LB streptomycin (Sm) from fecal samples on Day -2 of GFPT mice exhibit decreased GFP fluorescence. Culturing from the same samples on LB with both streptomycin and carbenicillin (Carb) suggests that for some mice, fluorescent colonies arising on LB streptomycin are Carb^S, *i.e.*, that they do not carry the CRISPR-Cas9 phagemid. Lack of fluorescent *E. coli* in fecal samples indicates eradication by carbenicillin where phage infection leading to colonization by Carb^R *E. coli* has not occurred. **(c)** Day 2 fecal suspensions from a subset of the mice (M1, M6, M10 for NT; M11, M16, M20 for GFPT) were cultured on larger plates for confirmation.

Figure S13. Flow cytometry plots of fecal samples for *in vivo* targeting of double-marked *E. coli* for all mice at all timepoints. Mice (n = 10 per group) were given either NT M13 (left) or GFPT M13 (right). Day -5, before engrafting *E. coli*; Day 0, after engraftment with double-marked GFP+ mCherry+ *E. coli*; Day -2, post phage and carbenicillin treatment; Day 7, one week post-phage and carbenicillin; Day -14, one week after removing carbenicillin from drinking water. Based on visual inspection, sample from Mouse 8 Day 0 was omitted from analyses.

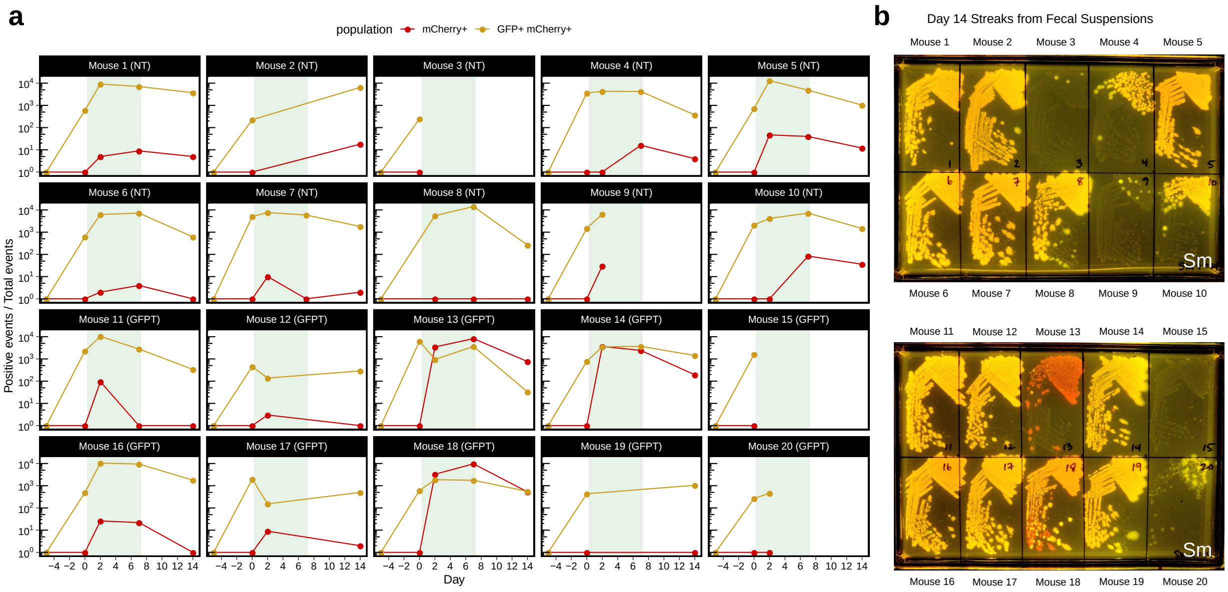

Figure S14. Doubly GFP+ mCherry+ and singly mCherry+ events by flow cytometry in fecal samples over time for individual mice in colonized with the double-marked strain under NT or GFPT conditions. (a) For each mouse, the number of doubly GFP+ mCherry+ events on Day -5 (before *E. coli* engraftment) was used to subtract GFP+ mCherry+ background for all subsequent timepoints, and the number of singly mCherry+ events on Day 0 (before phage treatment) was used to subtract mCherry+ background from all subsequent timepoints. Shaded green area indicates duration of carbenicillin treatment. Timepoints were excluded when both doubly GFP+ mCherry+ and singly mCherry+ events were below background thresholds, calculated as the respective highest observed background multiplied by a factor of 3. **(b)** Culture on LB with streptomycin from Day 14 fecal suspensions of mice treated with NT M13 (M1 to M10) and GFPT M13 (M11 to M20). Lack of fluorescent *E. coli* in fecal samples indicates eradication by carbenicillin where phage infection leading to colonization by Carb^R *E. coli* did not occur during the treatment phase.

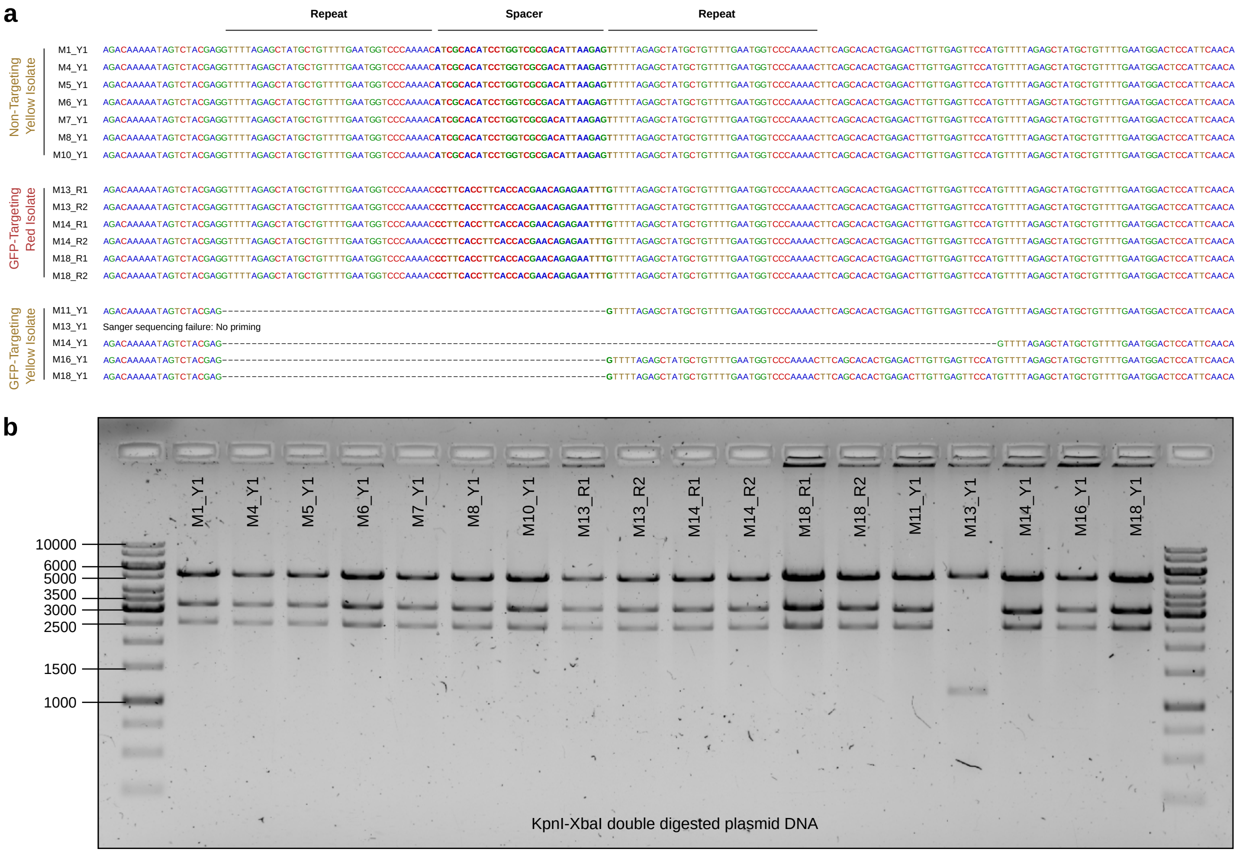

Figure S15. ***E. coli*** **isolates that remain double positive (GFP+ mCherry+) in fecal samples of mice treated with GFP-targeting M13 harbour CRISPR-Cas9 phagemids that exhibit loss of DNA. (a)** Sanger sequencing results confirm the expected spacer present in phagemid DNA extracted from fluorescent yellow isolates (Y1) colonizing NT mice (M1, M4, M5, M6, M7, M8, M10) and fluorescent red isolates (R1 and R2) colonizing GFPT mice (M13, M14, M18). In contrast, 4 of the 5 fluorescent yellow isolates colonizing GFPT mice (M11, M13, M14, M16, M18) were confirmed to have lost the spacer. No Sanger sequence data was obtained for the last isolate (M13) with report for failing being No Priming, suggesting loss of a larger fragment from the phagemid. **(b)** Diagnostic digest of CRISPR-Cas9 phagemid DNA confirms sizeable loss of phagemid DNA for the phagemid extracted from M13 Y1. Expected fragment sizes from KpnI-XbaI double digest: 5289, 3285, and 2573 bp.

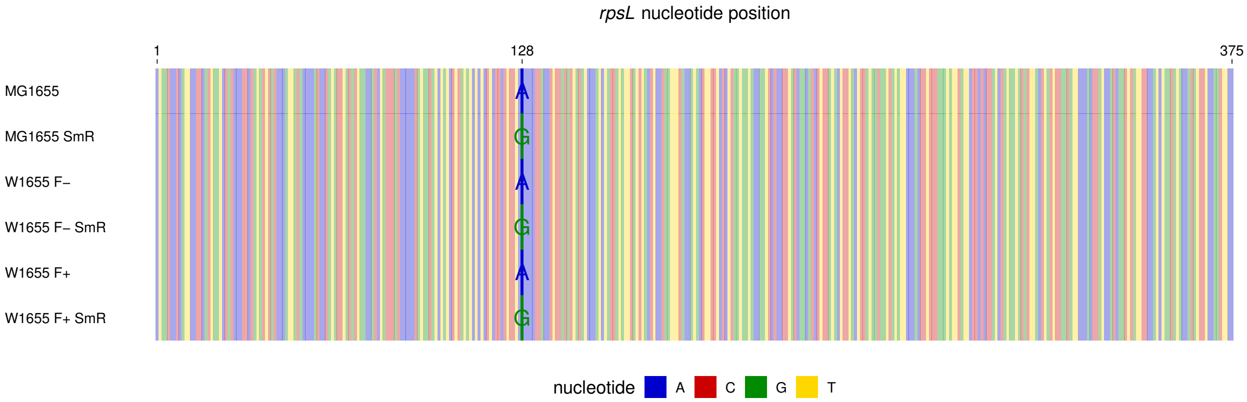

Figure S16. Confirmation of *rpsL*-Sm^R alleles by Sanger sequencing. The *rpsL* gene sequence is identical between *E. coli* MG1655, W1655 F−, and W1655 F+. Lambda Red recombineering was used to generate Sm^R derivatives of W1655 F− and W1655 F+ strains with identical alleles to MG1655 Sm^R, a spontaneous resistant mutant; all 3 were confirmed to have an A to G mutation at nucleotide 128 resulting in Lys42Arg.

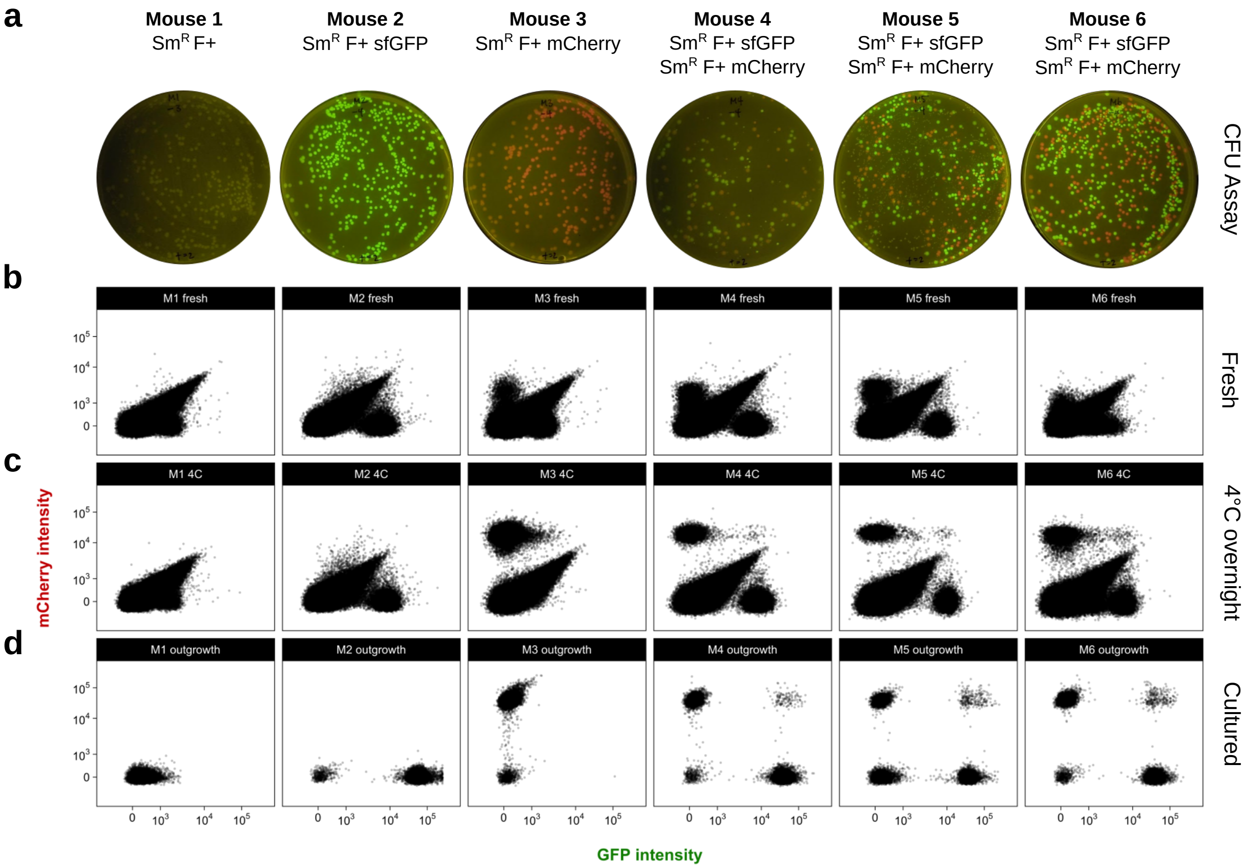

Figure S 17. Quantification of fluorescent *E. coli* in mouse fecal pellets by flow cytometry improves with overnight incubation of fecal suspensions at 4 °C. **(a)** Culture on LB streptomycin of fecal suspensions from streptomycin-treated mice colonized with non-fluorescent Sm^R *E. coli* W1655 F+ (Mouse 1), the GFP-marked (Mouse 2) or mCherry-marked derivative (Mouse 3), or both fluorescent strains (Mouse 4, 5, and 6). Flow cytometry was performed on fecal suspensions: **(b)** immediately after collecting, **(c)** overnight incubation at 4 °C, or **(d)** after inoculation in media and overnight culture.

Table S1. 16S rRNA gene sequencing indexing PCR primer sequences.

Name	PrimerSeq	Origin	IndexName	IndexSeq
F1_MetaIndex	AATGATACGGCGACCACCGAGATCTACACTATAGCCTTCGTCGGCAGCGTC	TruSeq i5	D501	TATAGCCT
F2_MetaIndex	AATGATACGGCGACCACCGAGATCTACACATAGAGGCTCGTCGGCAGCGTC	TruSeq i5	D502	ATAGAGGC
F3_MetaIndex	AATGATACGGCGACCACCGAGATCTACACCCTATCCTTCGTCGGCAGCGTC	TruSeq i5	D503	CCTATCCT
F4_MetaIndex	AATGATACGGCGACCACCGAGATCTACACGGCTCTGATCGTCGGCAGCGTC	TruSeq i5	D504	GGCTCTGA
F5_MetaIndex	AATGATACGGCGACCACCGAGATCTACACAGGCGAAGTCGTCGGCAGCGTC	TruSeq i5	D505	AGGCGAAG
F6_MetaIndex	AATGATACGGCGACCACCGAGATCTACACTAATCTTATCGTCGGCAGCGTC	TruSeq i5	D506	TAATCTTA
F7_MetaIndex	AATGATACGGCGACCACCGAGATCTACACCAGGACGTTCGTCGGCAGCGTC	TruSeq i5	D507	CAGGACGT
F8_MetaIndex	AATGATACGGCGACCACCGAGATCTACACGTACTGACTCGTCGGCAGCGTC	TruSeq i5	D508	GTACTGAC
F9_MetaIndex	AATGATACGGCGACCACCGAGATCTACACTGAACCTTTCGTCGGCAGCGTC	TruSeq Amplicon	A501	TGAACCTT
F10_MetaIndex	AATGATACGGCGACCACCGAGATCTACACTAGATCGCTCGTCGGCAGCGTC	Nextera i5	N501	TAGATCGC
F11_MetaIndex	AATGATACGGCGACCACCGAGATCTACACCTCTCTATTCGTCGGCAGCGTC	Nextera i5	N502	CTCTCTAT
F12_MetaIndex	AATGATACGGCGACCACCGAGATCTACACTATCCTCTTCGTCGGCAGCGTC	Nextera i5	N503	TATCCTCT
F13_MetaIndex	AATGATACGGCGACCACCGAGATCTACACAGAGTAGATCGTCGGCAGCGTC	Nextera i5	N504	AGAGTAGA
F14_MetaIndex	AATGATACGGCGACCACCGAGATCTACACGTAAGGAGTCGTCGGCAGCGTC	Nextera i5	N505	GTAAGGAG
F15_MetaIndex	AATGATACGGCGACCACCGAGATCTACACACTGCATATCGTCGGCAGCGTC	Nextera i5	N506	ACTGCATA
F16_MetaIndex	AATGATACGGCGACCACCGAGATCTACACAAGGAGTATCGTCGGCAGCGTC	Nextera i5	N507	AAGGAGTA
R13_MetaIndex	CAAGCAGAAGACGGCATACGAGATGTCGTGATGTCTCGTGGGCTCGG	TruSeq Amplicon	A701	ATCACGAC
R14_MetaIndex	CAAGCAGAAGACGGCATACGAGATCGAGTAATGTCTCGTGGGCTCGG	TruSeq i7	D701	ATTACTCG
R15_MetaIndex	CAAGCAGAAGACGGCATACGAGATTCTCCGGAGTCTCGTGGGCTCGG	TruSeq i7	D702	TCCGGAGA
R16_MetaIndex	CAAGCAGAAGACGGCATACGAGATAATGAGCGGTCTCGTGGGCTCGG	TruSeq i7	D703	CGCTCATT
R17_MetaIndex	CAAGCAGAAGACGGCATACGAGATGGAATCTCGTCTCGTGGGCTCGG	TruSeq i7	D704	GAGATTCC
R18_MetaIndex	CAAGCAGAAGACGGCATACGAGATTTCTGAATGTCTCGTGGGCTCGG	TruSeq i7	D705	ATTCAGAA
R19_MetaIndex	CAAGCAGAAGACGGCATACGAGATACGAATTCGTCTCGTGGGCTCGG	TruSeq i7	D706	GAATTCGT
R20_MetaIndex	CAAGCAGAAGACGGCATACGAGATAGCTTCAGGTCTCGTGGGCTCGG	TruSeq i7	D707	CTGAAGCT
R21_MetaIndex	CAAGCAGAAGACGGCATACGAGATGCGCATTAGTCTCGTGGGCTCGG	TruSeq i7	D708	TAATGCGC
R22_MetaIndex	CAAGCAGAAGACGGCATACGAGATCATAGCCGGTCTCGTGGGCTCGG	TruSeq i7	D709	CGGCTATG
R23_MetaIndex	CAAGCAGAAGACGGCATACGAGATTTCGCGGAGTCTCGTGGGCTCGG	TruSeq i7	D710	TCCGCGAA
R24_MetaIndex	CAAGCAGAAGACGGCATACGAGATGCGCGAGAGTCTCGTGGGCTCGG	TruSeq i7	D711	TCTCGCGC
R1_MetaIndex	CAAGCAGAAGACGGCATACGAGATTCGCCTTAGTCTCGTGGGCTCGG	Nextera i7	N701	TAAGGCGA
R2_MetaIndex	CAAGCAGAAGACGGCATACGAGATCTAGTACGGTCTCGTGGGCTCGG	Nextera i7	N702	CGTACTAG
R3_MetaIndex	CAAGCAGAAGACGGCATACGAGATTTCTGCCTGTCTCGTGGGCTCGG	Nextera i7	N703	AGGCAGAA
R4_MetaIndex	CAAGCAGAAGACGGCATACGAGATGCTCAGGAGTCTCGTGGGCTCGG	Nextera i7	N704	TCCTGAGC
R5_MetaIndex	CAAGCAGAAGACGGCATACGAGATAGGAGTCCGTCTCGTGGGCTCGG	Nextera i7	N705	GGACTCCT
R6_MetaIndex	CAAGCAGAAGACGGCATACGAGATCATGCCTAGTCTCGTGGGCTCGG	Nextera i7	N706	TAGGCATG
R7_MetaIndex	CAAGCAGAAGACGGCATACGAGATGTAGAGAGGTCTCGTGGGCTCGG	Nextera i7	N707	CTCTCTAC
R8_MetaIndex	CAAGCAGAAGACGGCATACGAGATCCTCTCTGGTCTCGTGGGCTCGG	Nextera i7	N708	CAGAGAGG
R25_MetaIndex	CAAGCAGAAGACGGCATACGAGATCTATCGCTGTCTCGTGGGCTCGG	TruSeq i7	D712	AGCGATAG
R10_MetaIndex	CAAGCAGAAGACGGCATACGAGATCAGCCTCGGTCTCGTGGGCTCGG	Nextera i7	N710	CGAGGCTG
R11_MetaIndex	CAAGCAGAAGACGGCATACGAGATTGCCTCTTGTCTCGTGGGCTCGG	Nextera i7	N711	AAGAGGCA
R12_MetaIndex	CAAGCAGAAGACGGCATACGAGATTCCTCTACGTCTCGTGGGCTCGG	Nextera i7	N712	GTAGAGGA

Table S2. 16S rRNA gene sequencing sample metadata.

Sample_ID	Index_ID	Index	Index2_ID	Index2	Sample_Well	Specimen	Timepoint	Sample_Type	Mouse	Day	chem_administration	host_body_product
exp11_M1_Pre-Sm	D706	GAATTCGT	D505	AGGCGAAG	E7	M1	Pre-Sm	Mouse	M1	-5		stool
exp11_M10_Pre-Sm	D704	GAGATTCC	N505	GTAAGGAG	F5	M10	Pre-Sm	Mouse	M10	-5		stool
exp11_M11_Pre-Sm	D709	CGGCTATG	D501	TATAGCCT	A10	M11	Pre-Sm	Mouse	M11	-5		stool
exp11_M12_Pre-Sm	D701	ATTACTCG	N504	AGAGTAGA	E2	M12	Pre-Sm	Mouse	M12	-5		stool
exp11_M13_Pre-Sm	D707	CTGAAGCT	D503	CCTATCCT	C8	M13	Pre-Sm	Mouse	M13	-5		stool
exp11_M14_Pre-Sm	D702	TCCGGAGA	N501	TAGATCGC	B3	M14	Pre-Sm	Mouse	M14	-5		stool
exp11_M15_Pre-Sm	D709	CGGCTATG	D505	AGGCGAAG	E10	M15	Pre-Sm	Mouse	M15	-5		stool
exp11_M16_Pre-Sm	D701	ATTACTCG	N506	ACTGCATA	G2	M16	Pre-Sm	Mouse	M16	-5		stool
exp11_M17_Pre-Sm	D708	TAATGCGC	D506	TAATCTTA	F9	M17	Pre-Sm	Mouse	M17	-5		stool
exp11_M18_Pre-Sm	D704	GAGATTCC	N501	TAGATCGC	B5	M18	Pre-Sm	Mouse	M18	-5		stool
exp11_M19_Pre-Sm	D702	TCCGGAGA	D505	AGGCGAAG	E3	M19	Pre-Sm	Mouse	M19	-5		stool
exp11_M2_Pre-Sm	D704	GAGATTCC	N506	ACTGCATA	G5	M2	Pre-Sm	Mouse	M2	-5		stool
exp11_M20_Pre-Sm	D703	CGCTCATT	N503	TATCCTCT	D4	M20	Pre-Sm	Mouse	M20	-5		stool
exp11_M21_Pre-Sm	D702	TCCGGAGA	D508	GTACTGAC	H3	M21	Pre-Sm	Mouse	M21	-5		stool
exp11_M22_Pre-Sm	A701	ATCACGAC	D507	CAGGACGT	H1	M22	Pre-Sm	Mouse	M22	-5		stool
exp11_M23_Pre-Sm	D704	GAGATTCC	D505	AGGCGAAG	E5	M23	Pre-Sm	Mouse	M23	-5		stool
exp11_M24_Pre-Sm	D704	GAGATTCC	A501	TGAACCTT	A5	M24	Pre-Sm	Mouse	M24	-5		stool
exp11_M3_Pre-Sm	A701	ATCACGAC	D508	GTACTGAC	H1	M3	Pre-Sm	Mouse	M3	-5		stool
exp11_M4_Pre-Sm	D701	ATTACTCG	N505	GTAAGGAG	F2	M4	Pre-Sm	Mouse	M4	-5		stool
exp11_M5_Pre-Sm	D706	GAATTCGT	N507	AAGGAGTA	G7	M5	Pre-Sm	Mouse	M5	-5		stool
exp11_M6_Pre-Sm	D705	ATTCAGAA	N502	CTCTCTAT	C6	M6	Pre-Sm	Mouse	M6	-5		stool
exp11_M7_Pre-Sm	D704	GAGATTCC	D506	TAATCTTA	F5	M7	Pre-Sm	Mouse	M7	-5		stool
exp11_M8_Pre-Sm	D705	ATTCAGAA	A501	TGAACCTT	A6	M8	Pre-Sm	Mouse	M8	-5		stool
exp11_M9_Pre-Sm	D707	CTGAAGCT	D505	AGGCGAAG	E8	M9	Pre-Sm	Mouse	M9	-5		stool
exp11_M1_Pre-Col	D708	TAATGCGC	D501	TATAGCCT	A9	M1	Post-Sm (Pre-Col)	Mouse	M1	-4	Streptomycin	stool
exp11_M10_Pre-Col	A701	ATCACGAC	N501	TAGATCGC	B1	M10	Post-Sm (Pre-Col)	Mouse	M10	-4	Streptomycin	stool
exp11_M11_Pre-Col	D702	TCCGGAGA	D503	CCTATCCT	C3	M11	Post-Sm (Pre-Col)	Mouse	M11	-4	Streptomycin	stool
exp11_M12_Pre-Col	D706	GAATTCGT	A501	TGAACCTT	A7	M12	Post-Sm (Pre-Col)	Mouse	M12	-4	Streptomycin	stool
exp11_M13_Pre-Col	D701	ATTACTCG	N507	AAGGAGTA	G2	M13	Post-Sm (Pre-Col)	Mouse	M13	-4	Streptomycin	stool
exp11_M14_Pre-Col	D703	CGCTCATT	N504	AGAGTAGA	E4	M14	Post-Sm (Pre-Col)	Mouse	M14	-4	Streptomycin	stool
exp11_M15_Pre-Col	D703	CGCTCATT	D505	AGGCGAAG	E4	M15	Post-Sm (Pre-Col)	Mouse	M15	-4	Streptomycin	stool
exp11_M16_Pre-Col	A701	ATCACGAC	N504	AGAGTAGA	E1	M16	Post-Sm (Pre-Col)	Mouse	M16	-4	Streptomycin	stool
exp11_M17_Pre-Col	A701	ATCACGAC	D502	ATAGAGGC	B1	M17	Post-Sm (Pre-Col)	Mouse	M17	-4	Streptomycin	stool
exp11_M18_Pre-Col	D703	CGCTCATT	D507	CAGGACGT	H4	M18	Post-Sm (Pre-Col)	Mouse	M18	-4	Streptomycin	stool
exp11_M19_Pre-Col	D702	TCCGGAGA	D501	TATAGCCT	A3	M19	Post-Sm (Pre-Col)	Mouse	M19	-4	Streptomycin	stool
exp11_M2_Pre-Col	D711	TCTCGCGC	D501	TATAGCCT	A12	M2	Post-Sm (Pre-Col)	Mouse	M2	-4	Streptomycin	stool
exp11_M20_Pre-Col	D711	TCTCGCGC	N507	AAGGAGTA	G12	M20	Post-Sm (Pre-Col)	Mouse	M20	-4	Streptomycin	stool
exp11_M21_Pre-Col	D704	GAGATTCC	D503	CCTATCCT	C5	M21	Post-Sm (Pre-Col)	Mouse	M21	-4	Streptomycin	stool
exp11_M22_Pre-Col	D701	ATTACTCG	N502	CTCTCTAT	C2	M22	Post-Sm (Pre-Col)	Mouse	M22	-4	Streptomycin	stool
exp11_M23_Pre-Col	D709	CGGCTATG	D508	GTACTGAC	H10	M23	Post-Sm (Pre-Col)	Mouse	M23	-4	Streptomycin	stool
exp11_M24_Pre-Col	D711	TCTCGCGC	D504	GGCTCTGA	D12	M24	Post-Sm (Pre-Col)	Mouse	M24	-4	Streptomycin	stool
exp11_M3_Pre-Col	D709	CGGCTATG	D504	GGCTCTGA	D10	M3	Post-Sm (Pre-Col)	Mouse	M3	-4	Streptomycin	stool
exp11_M4_Pre-Col	D706	GAATTCGT	N502	CTCTCTAT	C7	M4	Post-Sm (Pre-Col)	Mouse	M4	-4	Streptomycin	stool
exp11_M5_Pre-Col	D703	CGCTCATT	D502	ATAGAGGC	B4	M5	Post-Sm (Pre-Col)	Mouse	M5	-4	Streptomycin	stool
exp11_M6_Pre-Col	A701	ATCACGAC	N505	GTAAGGAG	F1	M6	Post-Sm (Pre-Col)	Mouse	M6	-4	Streptomycin	stool
exp11_M7_Pre-Col	D708	TAATGCGC	N507	AAGGAGTA	G9	M7	Post-Sm (Pre-Col)	Mouse	M7	-4	Streptomycin	stool
exp11_M8_Pre-Col	D704	GAGATTCC	N504	AGAGTAGA	E5	M8	Post-Sm (Pre-Col)	Mouse	M8	-4	Streptomycin	stool
exp11_M9_Pre-Col	D703	CGCTCATT	D503	CCTATCCT	C4	M9	Post-Sm (Pre-Col)	Mouse	M9	-4	Streptomycin	stool
exp11_M1_T-2	D704	GAGATTCC	N507	AAGGAGTA	G5	M1	Post-Col	Mouse	M1	-2	Streptomycin	stool
exp11_M10_T-2	D707	CTGAAGCT	N506	ACTGCATA	G8	M10	Post-Col	Mouse	M10	-2	Streptomycin	stool
exp11_M11_T-2	D701	ATTACTCG	D502	ATAGAGGC	B2	M11	Post-Col	Mouse	M11	-2	Streptomycin	stool
exp11_M12_T-2	D704	GAGATTCC	N502	CTCTCTAT	C5	M12	Post-Col	Mouse	M12	-2	Streptomycin	stool
exp11_M13_T-2	D704	GAGATTCC	D508	GTACTGAC	H5	M13	Post-Col	Mouse	M13	-2	Streptomycin	stool
exp11_M14_T-2	D710	TCCGCGAA	D505	AGGCGAAG	E11	M14	Post-Col	Mouse	M14	-2	Streptomycin	stool
exp11_M15_T-2	D702	TCCGGAGA	N507	AAGGAGTA	G3	M15	Post-Col	Mouse	M15	-2	Streptomycin	stool
exp11_M16_T-2	D710	TCCGCGAA	N507	AAGGAGTA	G11	M16	Post-Col	Mouse	M16	-2	Streptomycin	stool
exp11_M17_T-2	D706	GAATTCGT	D504	GGCTCTGA	D7	M17	Post-Col	Mouse	M17	-2	Streptomycin	stool
exp11_M18_T-2	D706	GAATTCGT	N503	TATCCTCT	D7	M18	Post-Col	Mouse	M18	-2	Streptomycin	stool
exp11_M19_T-2	D704	GAGATTCC	D502	ATAGAGGC	B5	M19	Post-Col	Mouse	M19	-2	Streptomycin	stool
exp11_M2_T-2	D701	ATTACTCG	A501	TGAACCTT	A2	M2	Post-Col	Mouse	M2	-2	Streptomycin	stool
exp11_M20_T-2	D701	ATTACTCG	N503	TATCCTCT	D2	M20	Post-Col	Mouse	M20	-2	Streptomycin	stool
exp11_M21_T-2	D706	GAATTCGT	D501	TATAGCCT	A7	M21	Post-Col	Mouse	M21	-2	Streptomycin	stool
exp11_M22_T-2	D704	GAGATTCC	N503	TATCCTCT	D5	M22	Post-Col	Mouse	M22	-2	Streptomycin	stool
exp11_M23_T-2	D708	TAATGCGC	D502	ATAGAGGC	B9	M23	Post-Col	Mouse	M23	-2	Streptomycin	stool
exp11_M24_T-2	A701	ATCACGAC	N503	TATCCTCT	D1	M24	Post-Col	Mouse	M24	-2	Streptomycin	stool
exp11_M3_T-2	D708	TAATGCGC	D508	GTACTGAC	H9	M3	Post-Col	Mouse	M3	-2	Streptomycin	stool
exp11_M4_T-2	D703	CGCTCATT	A501	TGAACCTT	A4	M4	Post-Col	Mouse	M4	-2	Streptomycin	stool
exp11_M5_T-2	A701	ATCACGAC	D501	TATAGCCT	A1	M5	Post-Col	Mouse	M5	-2	Streptomycin	stool
exp11_M6_T-2	A701	ATCACGAC	N502	CTCTCTAT	C1	M6	Post-Col	Mouse	M6	-2	Streptomycin	stool
exp11_M7_T-2	A701	ATCACGAC	N507	AAGGAGTA	G1	M7	Post-Col	Mouse	M7	-2	Streptomycin	stool
exp11_M8_T-2	D706	GAATTCGT	N504	AGAGTAGA	E7	M8	Post-Col	Mouse	M8	-2	Streptomycin	stool
exp11_M9_T-2	D706	GAATTCGT	D503	CCTATCCT	C7	M9	Post-Col	Mouse	M9	-2	Streptomycin	stool
exp11_M1_T0	D705	ATTCAGAA	D502	ATAGAGGC	B6	M1	T0	Mouse	M1	0	Streptomycin	stool
exp11_M10_T0	D707	CTGAAGCT	N504	AGAGTAGA	E8	M10	T0	Mouse	M10	0	Streptomycin	stool
exp11_M11_T0	D702	TCCGGAGA	D506	TAATCTTA	F3	M11	T0	Mouse	M11	0	Streptomycin	stool
exp11_M12_T0	D702	TCCGGAGA	A501	TGAACCTT	A3	M12	T0	Mouse	M12	0	Streptomycin	stool
exp11_M13_T0	D706	GAATTCGT	D508	GTACTGAC	H7	M13	T0	Mouse	M13	0	Streptomycin	stool
exp11_M14_T0	D711	TCTCGCGC	D503	CCTATCCT	C12	M14	T0	Mouse	M14	0	Streptomycin	stool
exp11_M15_T0	D701	ATTACTCG	D506	TAATCTTA	F2	M15	T0	Mouse	M15	0	Streptomycin	stool
exp11_M16_T0	D705	ATTCAGAA	N503	TATCCTCT	D6	M16	T0	Mouse	M16	0	Streptomycin	stool
exp11_M17_T0	D705	ATTCAGAA	D508	GTACTGAC	H6	M17	T0	Mouse	M17	0	Streptomycin	stool
exp11_M18_T0	D711	TCTCGCGC	D502	ATAGAGGC	B12	M18	T0	Mouse	M18	0	Streptomycin	stool
exp11_M19_T0	D708	TAATGCGC	D504	GGCTCTGA	D9	M19	T0	Mouse	M19	0	Streptomycin	stool
exp11_M2_T0	D706	GAATTCGT	N501	TAGATCGC	B7	M2	T0	Mouse	M2	0	Streptomycin	stool
exp11_M20_T0	D703	CGCTCATT	N506	ACTGCATA	G4	M20	T0	Mouse	M20	0	Streptomycin	stool
exp11_M21_T0	D701	ATTACTCG	D505	AGGCGAAG	E2	M21	T0	Mouse	M21	0	Streptomycin	stool
exp11_M22_T0	D703	CGCTCATT	N501	TAGATCGC	B4	M22	T0	Mouse	M22	0	Streptomycin	stool
exp11_M23_T0	D707	CTGAAGCT	D504	GGCTCTGA	D8	M23	T0	Mouse	M23	0	Streptomycin	stool
exp11_M24_T0	D710	TCCGCGAA	D506	TAATCTTA	F11	M24	T0	Mouse	M24	0	Streptomycin	stool
exp11_M3_T0	D701	ATTACTCG	D508	GTACTGAC	H2	M3	T0	Mouse	M3	0	Streptomycin	stool
exp11_M4_T0	D706	GAATTCGT	D507	CAGGACGT	H7	M4	T0	Mouse	M4	0	Streptomycin	stool
exp11_M5_T0	D709	CGGCTATG	D502	ATAGAGGC	B10	M5	T0	Mouse	M5	0	Streptomycin	stool
exp11_M6_T0	D707	CTGAAGCT	N503	TATCCTCT	D8	M6	T0	Mouse	M6	0	Streptomycin	stool
exp11_M7_T0	D704	GAGATTCC	D501	TATAGCCT	A5	M7	T0	Mouse	M7	0	Streptomycin	stool
exp11_M8_T0	D710	TCCGCGAA	D503	CCTATCCT	C11	M8	T0	Mouse	M8	0	Streptomycin	stool
exp11_M9_T0	D703	CGCTCATT	D501	TATAGCCT	A4	M9	T0	Mouse	M9	0	Streptomycin	stool
exp11_M1_T1	D705	ATTCAGAA	N507	AAGGAGTA	G6	M1	T1	Mouse	M1	1	Streptomycin, Carbenicillin	stool
exp11_M10_T1	D707	CTGAAGCT	A501	TGAACCTT	A8	M10	T1	Mouse	M10	1	Streptomycin, Carbenicillin	stool
exp11_M11_T1	D701	ATTACTCG	D501	TATAGCCT	A2	M11	T1	Mouse	M11	1	Streptomycin, Carbenicillin	stool
exp11_M12_T1	D701	ATTACTCG	D507	CAGGACGT	H2	M12	T1	Mouse	M12	1	Streptomycin, Carbenicillin	stool
exp11_M13_T1	D705	ATTCAGAA	D506	TAATCTTA	F6	M13	T1	Mouse	M13	1	Streptomycin, Carbenicillin	stool
exp11_M14_T1	D710	TCCGCGAA	D504	GGCTCTGA	D11	M14	T1	Mouse	M14	1	Streptomycin, Carbenicillin	stool
exp11_M15_T1	D703	CGCTCATT	D504	GGCTCTGA	D4	M15	T1	Mouse	M15	1	Streptomycin, Carbenicillin	stool
exp11_M16_T1	D701	ATTACTCG	N501	TAGATCGC	B2	M16	T1	Mouse	M16	1	Streptomycin, Carbenicillin	stool
exp11_M17_T1	A701	ATCACGAC	D503	CCTATCCT	C1	M17	T1	Mouse	M17	1	Streptomycin, Carbenicillin	stool
exp11_M18_T1	D707	CTGAAGCT	N501	TAGATCGC	B8	M18	T1	Mouse	M18	1	Streptomycin, Carbenicillin	stool
exp11_M19_T1	D705	ATTCAGAA	D504	GGCTCTGA	D6	M19	T1	Mouse	M19	1	Streptomycin, Carbenicillin	stool
exp11_M2_T1	D710	TCCGCGAA	D508	GTACTGAC	H11	M2	T1	Mouse	M2	1	Streptomycin, Carbenicillin	stool
exp11_M20_T1	D710	TCCGCGAA	D501	TATAGCCT	A11	M20	T1	Mouse	M20	1	Streptomycin, Carbenicillin	stool
exp11_M21_T1	D703	CGCTCATT	D508	GTACTGAC	H4	M21	T1	Mouse	M21	1	Streptomycin, Carbenicillin	stool
exp11_M22_T1	D704	GAGATTCC	D507	CAGGACGT	H5	M22	T1	Mouse	M22	1	Streptomycin, Carbenicillin	stool
exp11_M23_T1	A701	ATCACGAC	D505	AGGCGAAG	E1	M23	T1	Mouse	M23	1	Streptomycin, Carbenicillin	stool
exp11_M24_T1	D702	TCCGGAGA	N503	TATCCTCT	D3	M24	T1	Mouse	M24	1	Streptomycin, Carbenicillin	stool
exp11_M3_T1	D708	TAATGCGC	D505	AGGCGAAG	E9	M3	T1	Mouse	M3	1	Streptomycin, Carbenicillin	stool
exp11_M4_T1	D707	CTGAAGCT	N505	GTAAGGAG	F8	M4	T1	Mouse	M4	1	Streptomycin, Carbenicillin	stool
exp11_M5_T1	D709	CGGCTATG	D503	CCTATCCT	C10	M5	T1	Mouse	M5	1	Streptomycin, Carbenicillin	stool
exp11_M6_T1	D702	TCCGGAGA	N502	CTCTCTAT	C3	M6	T1	Mouse	M6	1	Streptomycin, Carbenicillin	stool
exp11_M7_T1	D707	CTGAAGCT	D502	ATAGAGGC	B8	M7	T1	Mouse	M7	1	Streptomycin, Carbenicillin	stool
exp11_M8_T1	D706	GAATTCGT	N506	ACTGCATA	G7	M8	T1	Mouse	M8	1	Streptomycin, Carbenicillin	stool
exp11_M9_T1	D704	GAGATTCC	D504	GGCTCTGA	D5	M9	T1	Mouse	M9	1	Streptomycin, Carbenicillin	stool
exp11_M1_T2	D707	CTGAAGCT	N507	AAGGAGTA	G8	M1	T2	Mouse	M1	2	Streptomycin, Carbenicillin	stool
exp11_M10_T2	D702	TCCGGAGA	N505	GTAAGGAG	F3	M10	T2	Mouse	M10	2	Streptomycin, Carbenicillin	stool
exp11_M11_T2	A701	ATCACGAC	D504	GGCTCTGA	D1	M11	T2	Mouse	M11	2	Streptomycin, Carbenicillin	stool
exp11_M12_T2	D705	ATTCAGAA	D507	CAGGACGT	H6	M12	T2	Mouse	M12	2	Streptomycin, Carbenicillin	stool
exp11_M13_T2	D702	TCCGGAGA	D504	GGCTCTGA	D3	M13	T2	Mouse	M13	2	Streptomycin, Carbenicillin	stool
exp11_M14_T2	D711	TCTCGCGC	D506	TAATCTTA	F12	M14	T2	Mouse	M14	2	Streptomycin, Carbenicillin	stool
exp11_M15_T2	D705	ATTCAGAA	D505	AGGCGAAG	E6	M15	T2	Mouse	M15	2	Streptomycin, Carbenicillin	stool
exp11_M16_T2	D703	CGCTCATT	N505	GTAAGGAG	F4	M16	T2	Mouse	M16	2	Streptomycin, Carbenicillin	stool
exp11_M17_T2	D707	CTGAAGCT	D506	TAATCTTA	F8	M17	T2	Mouse	M17	2	Streptomycin, Carbenicillin	stool
exp11_M18_T2	A701	ATCACGAC	A501	TGAACCTT	A1	M18	T2	Mouse	M18	2	Streptomycin, Carbenicillin	stool
exp11_M19_T2	D706	GAATTCGT	D506	TAATCTTA	F7	M19	T2	Mouse	M19	2	Streptomycin, Carbenicillin	stool
exp11_M2_T2	D702	TCCGGAGA	N504	AGAGTAGA	E3	M2	T2	Mouse	M2	2	Streptomycin, Carbenicillin	stool
exp11_M20_T2	D706	GAATTCGT	N505	GTAAGGAG	F7	M20	T2	Mouse	M20	2	Streptomycin, Carbenicillin	stool
exp11_M21_T2	D705	ATTCAGAA	D503	CCTATCCT	C6	M21	T2	Mouse	M21	2	Streptomycin, Carbenicillin	stool
exp11_M22_T2	D702	TCCGGAGA	N506	ACTGCATA	G3	M22	T2	Mouse	M22	2	Streptomycin, Carbenicillin	stool
exp11_M23_T2	D703	CGCTCATT	D506	TAATCTTA	F4	M23	T2	Mouse	M23	2	Streptomycin, Carbenicillin	stool
exp11_M24_T2	D711	TCTCGCGC	D505	AGGCGAAG	E12	M24	T2	Mouse	M24	2	Streptomycin, Carbenicillin	stool
exp11_M3_T2	D707	CTGAAGCT	D508	GTACTGAC	H8	M3	T2	Mouse	M3	2	Streptomycin, Carbenicillin	stool
exp11_M4_T2	D705	ATTCAGAA	N505	GTAAGGAG	F6	M4	T2	Mouse	M4	2	Streptomycin, Carbenicillin	stool
exp11_M5_T2	D707	CTGAAGCT	D501	TATAGCCT	A8	M5	T2	Mouse	M5	2	Streptomycin, Carbenicillin	stool
exp11_M6_T2	D702	TCCGGAGA	D507	CAGGACGT	H3	M6	T2	Mouse	M6	2	Streptomycin, Carbenicillin	stool
exp11_M7_T2	A701	ATCACGAC	D506	TAATCTTA	F1	M7	T2	Mouse	M7	2	Streptomycin, Carbenicillin	stool
exp11_M8_T2	D705	ATTCAGAA	N501	TAGATCGC	B6	M8	T2	Mouse	M8	2	Streptomycin, Carbenicillin	stool
exp11_M9_T2	D708	TAATGCGC	D503	CCTATCCT	C9	M9	T2	Mouse	M9	2	Streptomycin, Carbenicillin	stool
exp11_CTRL_STD_Zymo_mixture_1	D709	CGGCTATG	N507	AAGGAGTA	G10	Zymo Mix 1	NA	CTRL_Zymo	NA	NA		
exp11_CTRL_STD_Zymo_mixture_2	D707	CTGAAGCT	D507	CAGGACGT	H8	Zymo Mix 2	NA	CTRL_Zymo	NA	NA		
exp11_CTRL_STD_Zymo_DNA	D708	TAATGCGC	A501	TGAACCTT	A9	Zymo DNA	NA	CTRL_Zymo	NA	NA		
exp11_NTC_1	D708	TAATGCGC	N501	TAGATCGC	B9	NTC	NA	CTRL_NTC	NA	NA		
exp11_NTC_2	D708	TAATGCGC	N502	CTCTCTAT	C9	NTC	NA	CTRL_NTC	NA	NA		
exp11_NTC_3	D708	TAATGCGC	N503	TATCCTCT	D9	NTC	NA	CTRL_NTC	NA	NA		
exp11_NTC_4	D708	TAATGCGC	N504	AGAGTAGA	E9	NTC	NA	CTRL_NTC	NA	NA		
exp11_NTC_5	D708	TAATGCGC	N505	GTAAGGAG	F9	NTC	NA	CTRL_NTC	NA	NA		
exp11_NTC_6	D708	TAATGCGC	N506	ACTGCATA	G9	NTC	NA	CTRL_NTC	NA	NA		
exp11_NTC_7	D708	TAATGCGC	D507	CAGGACGT	H9	NTC	NA	CTRL_NTC	NA	NA		
exp11_CTRL_NEG_no_feces_4	D701	ATTACTCG	D504	GGCTCTGA	D2	CTRL_NEG_no_feces_4	NA	CTRL_NEG	NA	NA		
exp11_CTRL_NEG_no_feces_5	D702	TCCGGAGA	D502	ATAGAGGC	B3	CTRL_NEG_no_feces_5	NA	CTRL_NEG	NA	NA		
exp11_CTRL_NEG_no_feces_3	D703	CGCTCATT	N507	AAGGAGTA	G4	CTRL_NEG_no_feces_3	NA	CTRL_NEG	NA	NA		
exp11_CTRL_NEG_1	D705	ATTCAGAA	D501	TATAGCCT	A6	CTRL_NEG_1	NA	CTRL_NEG	NA	NA		
exp11_CTRL_NEG_no_feces_1	D706	GAATTCGT	D502	ATAGAGGC	B7	CTRL_NEG_no_feces_1	NA	CTRL_NEG	NA	NA		
exp11_CTRL_NEG_no_feces_2	D709	CGGCTATG	D506	TAATCTTA	F10	CTRL_NEG_no_feces_2	NA	CTRL_NEG	NA	NA		
exp11_CTRL_NEG_no_feces_9	D710	TCCGCGAA	D502	ATAGAGGC	B11	CTRL_NEG_no_feces_9	NA	CTRL_NEG	NA	NA		
exp11_CTRL_NEG_no_feces_7	D711	TCTCGCGC	D508	GTACTGAC	H12	CTRL_NEG_no_feces_7	NA	CTRL_NEG	NA	NA		
exp11_CTRL_NEG_2	A701	ATCACGAC	N506	ACTGCATA	G1	CTRL_NEG_2	NA	CTRL_NEG	NA	NA		
exp11_CTRL_NEG_no_feces_10	D703	CGCTCATT	N502	CTCTCTAT	C4	CTRL_NEG_no_feces_10	NA	CTRL_NEG	NA	NA		
exp11_CTRL_NEG_no_feces_6	D705	ATTCAGAA	N504	AGAGTAGA	E6	CTRL_NEG_no_feces_6	NA	CTRL_NEG	NA	NA		
exp11_CTRL_NEG_no_feces_8	D705	ATTCAGAA	N506	ACTGCATA	G6	CTRL_NEG_no_feces_8	NA	CTRL_NEG	NA	NA		
exp11_CTRL_STD_human_feces_1	D701	ATTACTCG	D503	CCTATCCT	C2	Human 1	NA	CTRL_Human	NA	NA		stool
exp11_CTRL_STD_human_feces_2	D707	CTGAAGCT	N502	CTCTCTAT	C8	Human 2	NA	CTRL_Human	NA	NA		stool

Word Count

```
File: main.tex
Encoding: ascii
Sum count: 6438
Words in text: 5083
Words in headers: 40
Words outside text (captions, etc.): 1315
Number of headers: 11
Number of floats/tables/figures: 5
Number of math inlines: 0
Number of math displayed: 0
Subcounts:
  text+headers+captions (#headers/#floats/#inlines/#displayed)
  1+0+0 (0/0/0/0) Subsection
  932+1+0 (1/0/0/0) Section: Introduction
  0+1+0 (1/0/0/0) Section: Results
  1182+12+337 (1/1/0/0) Subsection: Phage M13 can be used to deliver DNA to \Ecoli in the gut
  975+5+431 (1/2/0/0) Subsection: M13 carrying CRISPR-Cas9 can target \Ecoli \invitro
  446+6+307 (1/1/0/0) Subsection: Sequence-specific depletion of \Ecoli \invivo using M13-delivered CRISPR-Cas9
  550+6+240 (1/1/0/0) Subsection: M13-delivered CRISPR-Cas9 can induce chromosomal deletions \invivo
  610+1+0 (1/0/0/0) Section: Discussion
  130+1+0 (1/0/0/0) Section: Acknowledgments
  103+2+0 (1/0/0/0) Section: Author Contributions
  115+1+0 (1/0/0/0) Section: Funding
  39+4+0 (1/0/0/0) Section: Conflict of Interest Statement
```